Abolafia-Rosenzweig Ronnie (Orcid ID: 0000-0002-6169-6430)
He Cenlin (Orcid ID: 0000-0002-7367-2815)

Hydrological Processes

Quantifying the impacts of fire-related perturbations in WRF-Hydro terrestrial water budget simulations in California's Feather River Basin

Ronnie Abolafia-Rosenzweig [1], David Gochis [2], Andrew Schwarz [3], Thomas H. Painter [2], Jeffery Deems [2], Aubrey Dugger [1], Matthew Casali [1], Cenlin He [1]

[1] NSF National Center for Atmospheric Research, Boulder, Colorado, USA

[2] Airborne Snow Observatories, Inc.

[3] California Department of Water Resources

Corresponding Author: abolafia@ucar.edu

Data and Code Availability

WRF-Hydro input and output data used to support the findings of this study are publicly available on Zenodo (Abolafia-Rosenzweig et al., 2024a). The widely used WRF-Hydro modeling system used in this study is publicly available on GitHub: https://github.com/NCAR/wrf_hydro_nwm_public. Updated WRF-Hydro files using the fire-aware snow albedo parameterization are publicly available on GitHub: https://github.com/RAbolafiaRosenzweig/WRF-Hydro-BATS_fire_enhanced_snow_albedo_degradation. Data processing and visualization MATLAB scripts are available on GitHub: https://github.com/RAbolafiaRosenzweig/WRF-Hydro_FireSensitvity_FeatherRiver. ASO survey data can be accessed here: https://data.airbornesnowobservatories.com/. In-situ streamflow data used in this study is made publicly by the California Data Exchange Center (https://cdec.water.ca.gov/).

Conflict of Interest

The authors declare no conflicts of interest relevant to this study.

This is the author manuscript accepted for publication and has undergone full peer review but has not been through the copyediting, typesetting, pagination and proofreading process, which may lead to differences between this version and the Version of Record. Please cite this article as doi: 10.1002/hyp.15314

Abstract

Wildfire activity in the western United States (WUS) is increasingly impacting water supply, and land surface models (LSMs) that do not explicitly account for fire disturbances can have critical uncertainties in burned areas. This study quantified responses from the Weather Research and Forecasting Hydrological modeling system (WRF-Hydro) to a suite of fire-related perturbations to hydrologic soil and runoff parameters, vegetation area, land cover classifications and associated vegetation properties, and snow albedo across the heavily burned Feather River Basin in California. These experiments were used to quantify the impacts of fire-related perturbations in model simulations under the observed meteorological conditions during the 2000-2022 water years and determine whether applying these fire-related perturbations enhanced post-fire model accuracy across the 11-12 post-fire months evaluated herein. The most comprehensive fire-aware simulation consistently modelled enhanced annual catchment streamflow (by 8-37%), subsurface flow (by 72-116%), and soil moisture (by 4-9%), relative to the *baseline* simulation which neglected fire impacts. Simulated fire-enhanced streamflow was predominately attributable to fire-induced vegetation area reductions that reduced transpiration. Simulated streamflow enhancements occurred throughout the water year, excluding early-summer (e.g., May-June) when the *baseline* simulation modelled relatively more snowmelt and streamflow because fire perturbations caused earlier model snow depletion. Vegetation area reductions favoured increased model ground snow accumulation and enhanced snow ablation while imposed snow albedo darkening perturbations enhanced ablation, ultimately resulting in similar peak SWE and earlier snow disappearance (on average by 8-days) from the most comprehensive fire-aware simulation relative to the *baseline* simulation. The *baseline* simulation had large degradations in streamflow accuracy following major fire events that were likely partially attributable to neglecting fire disturbances. Applying fire-related perturbations reduced post-fire streamflow anomaly biases across the three study catchments. However, remaining large post-fire streamflow uncertainties in the fire-perturbed simulation underscores the importance of additional observationally constrained fire-disturbance model developments.

Keywords: Land surface model, fire, hydrology, streamflow, snow, WRF-Hydro, Noah-MP

1. INTRODUCTION

Seasonal snowpack serves as a natural water reservoir in the western United States (WUS) where most of the streamflow originates as snow (Viviroli et al., 2007; Li et al., 2017; Kapnick et al., 2018). Rising trends in wildfire burn area over snowy WUS regions (255 km^2/year from 1984-2020; Abolafia-Rosenzweig et al., 2022a) are increasingly impacting water supply in headwater catchments (Williams et al., 2022; Koshkin et al., 2022; Smoot and Gleason, 2021; Kampf et al., 2022). The growing impact of wildfire on water supply is projected to increase over the next few decades with climate projections showing 2021-2050 being twice as conducive for WUS wildfires compared to 1991-2020 (Abatzoglou et al., 2021; Williams et al., 2022). Failure to account for fire perturbations in hydrologic and land surface models (LSMs) that are used to inform water resources management can result in significant post-fire inaccuracies (Abolafia-Rosenzweig et el., 2024b) and potential water resource mismanagement. Therefore, it is increasingly important to evaluate model sensitives to fire-related land cover disturbances and account for these impacts on water supply in models used to inform water management decisions across the WUS.

Fire impacts on land surface hydrology are associated with complex soil-vegetation-hydrology-meteorology interactions through fire-induced alterations to soil hydrologic properties and the destruction and charring of vegetation. A suite of analyses have leveraged in-situ and remote sensing observations to quantify impacts of fire-related disturbances to streamflow (Q), evapotranspiration (ET), infiltration and soil moisture (SM), and snowpack (Hampton and Basu, 2022; Harpold et al., 2014; Kampf et al., 2022; Koshkin et al., 2022; Smoot and Gleason, 2021; Goeking and Tarboton, 2022; Spence et al., 2020; Niemeyer et al., 2020; Stoof et al., 2012; Shakesby and Doerr, 2006; Martin and Moody, 2001; Moody et al., 2008; Ebel and Martin, 2017; Ebel, 2020; Gleason et al., 2013, 2019; Ahmad et al., 2024). Fire impacts on the terrestrial water budget are often associated with reduced infiltration, enhanced Q, reduced ET, greater ground snow accumulation and enhanced snow ablation favoring earlier spring snowmelt and snow disappearance. However, there is substantial spatiotemporal heterogeneity in fire-disturbance impacts on hydrology which are dependent on interactions among many factors including: burn area and severity, catchment size, human management, vegetation, soil properties, meteorology, and topography (Pugh and Gordon 2013; Goeking and Tarboton 2020, 2022; Spence et al., 2020; Niemeyer et al., 2020; Atchley et al., 2018; Partington et al., 2022; Ahmad et al., 2024). Thus, simulating post-fire hydrology requires accurate representation of fire disturbances to the land surface in sophisticated models that accurately represent soil-vegetation-meteorology-hydrology interactions.

Fire effects on soil—increased bulk density, reduced pore space, and formation of a hydrophobic layer at the soil surface—are generally associated with lower infiltration, drier topsoil, wetter subsoil and higher runoff efficiency (Abolafia-Rosenzweig et al., 2024b; Stoof et al., 2012; Shakesby and Doerr, 2006; Martin and Moody, 2001; Moody et al., 2008; Ebel and Martin, 2017; Ebel, 2020). Burning of vegetation often has competing impacts on snow and streamflow. For instance, vegetation burning contributes to greater ground snow accumulation by reducing downward longwave radiation and precipitation interception (Seibert et al., 2010; Harpold et al., 2014; Burles and Boon, 2011). Conversely, vegetation burning can favour faster snow ablation and less snowpack through snow darkening from burned debris and soot shedding from standing trees onto the snowpack, reduced shading, and increased wind speeds and associated increases to turbulent heat flux to the snowpack (Seibert et al., 2010; Harpold et al., 2014; Pugh and Small, 2012; Burles and Boon, 2011; Gleason et al., 2013, 2019; Niemeyer et al., 2020; Maxwell and St Clair, 2019; Kampf et al., 2022). Vegetation removal also has competing effects on ET through decreased transpiration and canopy interception but increased bare ground evaporation (Bond-Lamberty et al., 2009; Maina and Siirila-Woodburm, 2020; Abolafia-Rosenzweig et al., 2024b).

Previous studies have attempted to account for fire impacts on hydrology in simple hydrological models (e.g., curve number-based); however, these approaches generally had insufficient performance or were only able to provide adequate results for specific variables (e.g., peak flow) at calibrated watersheds (Chen et al., 2013; Kinoshita et al., 2014; Wang et al., 2020). This motivates a sophisticated physically-based approach to post-fire hydrologic modeling, allowing in-depth mechanistic analyses that account for complex fire impacts on hydrology. Recent modeling analyses have begun to address this gap by quantifying fire induced uncertainties in physically-based LSM simulations (Abolafia-Rosenzweig et al., 2024) and explicitly accounting for fire-related perturbations in these models (Atchley et al., 2018; Li et al., 2023; Wang et al., 2020; Maina and Siirila-Woodburn, 2020; Kumar et al., 2021). These analyses have accounted for fire-induced increases to surface soil hydrophobicity and vegetation removal by perturbing soil hydrologic properties and vegetation parameters and assimilating remotely sensed fire signatures. Namely, surface soil hydrophobicity has been accounted for in previous modeling studies by applying observationally informed empirical perturbations to the surface soil saturated hydraulic conductivity (K_{sat}) (Robichaud, 2000; Blake et al., 2009; Ebel and Martin, 2017; Moody et al., 2015) which controls the infiltration rate, or by recalibrating a model to more accurately simulate observed post-fire streamflow (Li et al., 2022). Fire-induced vegetation reductions

have been accounted for by informing model simulations with observed reductions to leaf area index (LAI), vegetation height, vegetation optical depth, and imposing shifts to land cover classifications over burned areas (e.g., forested to barren and sparsely vegetated) (Atchley et al., 2018; Li et al., 2022; Wang et al., 2020; Maina and Siirila-Woodburn, 2020; Kumar et al., 2021).

The overarching goals of these previous modeling studies were to: (i) quantify changes in model skill following major fire events, (ii) quantify fire impacts on hydrology by comparing a baseline simulation that does not account for fire impacts with a fire-aware simulation that imposes fire-related perturbations, and (iii) determine if accounting for fire perturbations improves post-fire model accuracy. The approach for objective (ii) is akin to earlier paired catchment studies (e.g., Stoof et al., 2012), where a no-fire simulation is used to represent a twin unburned catchment, and the fire-aware simulation represents the fire-perturbed catchment. Previous model-based research found that imposing fire-related perturbations to model simulations decreased simulated ET while enhancing surface water flow and snow accumulation, with the magnitude and timing of these impacts largely depending on meteorological conditions (Atchley et al., 2018; Li et al., 2022; Wang et al., 2020; Maina and Siirila-Woodburn, 2020). Failure to adequately account for fire disturbances increases LSM uncertainty after major fire events (Abolafia-Rosenzweig et al., 2024b), whereas accounting for fire perturbations can enhance post-fire model accuracy for Q and ET (Wang et al., 2020; Kumar et al., 2021 and Li et al., 2022). However, these previous modeling studies have relied on domain-specific calibration or data assimilation and have been performed over a small sample of study domains. Thus, further research is valuable to work towards the development of a generalizable fire-disturbance scheme applicable to hydrological forecasting systems can improve model accuracy across a range of fire-impacted domains that are crucial for water and food security.

In this contemporary early-stage of physically-based post-fire land surface model development there is a growing need to quantify the impacts of fire disturbances in model simulations across a range of fire prone landscapes and evaluate whether accounting for these perturbations alters post-fire model accuracy. Important gaps in this area of research are a lack of: (a) quantifications of simulated water budget responses to incrementally applied fire-related perturbations, (2) evaluations across a range of burned snow-dominated areas which are critically important for water supply, and (3) evaluations using operational model systems and configurations which can inform water management forecasting systems. This study addresses these gaps by: (i) quantifying the impacts of fire-related perturbations in

simulations from the operationally used WRF-Hydro modeling system across the heavily burned and snow-dominated Feather River Basin, and (ii) evaluating whether explicitly accounting for fire perturbations in WRF-Hydro alters simulated post-fire streamflow accuracy.

2. Data and Methods

2.1 Study Domain

This study focused on three recently burned catchments in the Feather River Basin: East Branch North Fork Feather (EBNFF), Middle Fork Feather (MFF), and North Fork Feather (NFF) (Figure 1). The Feather River basin is the primary river basin for the California State Water Project. Of the Basin's 2.3 million acres, almost 1.6 million acres burned between 2018 and 2022. As the source watershed for the State Water Project, fire related impacts to hydrology could cause significant impacts to water supply operations and deliveries to the 27 million Californians that receive State Water Project supplies. From 2018-2022, the following major fire events burned across the three study catchments in the Feather River Basin: (i) Camp Fire which was ignited in November 2018 and burned 153,336 acres (240 square miles); (ii) North Complex Fire which was ignited in August 2020 and burned 318,776 acres (498 square miles); (iii) Dixie Fire which was ignited in July 2021 and burned 963,309 acres (1,505 square miles); (iv) Sugar Fire which was ignited in July 2021 and burned 105,076 acres (164 square miles); and (v) Walker Fire which was ignited in September 2019 and burned 54,628 acres (85 square miles). There has also been burning in the study domain excluding these major fire events. Specifically, the 2000-2022 total burn area excluding the study fire events sums to 24% of the cumulative burn area of the 5 study fire events (Figure S1) which may partially confound pre- to post-fire model skill comparisons (Section 2.3 and 3.1) because there is no true pre-fire period with negligible burning. Streamflow analyses for these three burned catchments are conducted at California Department of Water Resources (CADWR) stream gauge stations near catchment outlets which include: (i) North Fork Feather River at Pulga (NFP) for the NFF catchment; (ii) Indian Creek below Indian Falls (ICR) for the EBNFF catchment; and (iii) Feather River at Merrimac (MER) for the MFF catchment (Figure 1). Streamflow data from the NFP, ICR and MER stations began in the 2005, 2007 and 1997 water years, respectively. Although human management, such as diversions, are likely to impact streamflow at times, we did not explicitly consider human impacts in model simulations. Therefore, inconsistencies between

simulations and observations may be partially attributable to neglect of human impacts along with other uncertainty sources including meteorological forcing, land surface input parameters, and model physics.

The three study catchments have complex topography with minimum catchment elevations ranging from 129 – 799 m and maximum elevations ranging from 2402 – 2741 m. Winter is the wettest season in each study catchment, with 51-52% of mean annual precipitation (mean annual precipitation = 785, 1033 and 1239 mm in EBNFF, MFF and NFF, respectively) falling from December – February when mean catchment temperatures are near-zero (0.3 – 1.8°C). Thirty-three to thirty-six percent of annual precipitation fell as snow across the study domain and only 2-3% of the annual precipitation occurs during summer months (June – August) when human water demands tend to be greatest, highlighting the importance of prudently storing and managing winter precipitation and snowmelt. Fall (September–November) and Spring (March–May) snowfall are also valuable components of the catchment-scale water resources, with 46% of annual precipitation received during Fall and Spring and 15-16% and 35-39% of this precipitation coming as snowfall, respectively.

2.2 WRF-Hydro experiments

Simulations were generated over the study domain using the community Weather Research and Forecasting Hydrological modeling system (WRF-Hydro; Gochis et al., 2020) which is an open-source physics-based multi-spatial community model that relies on the Noah-MP LSM (Niu et al., 2011; He et al., 2023) to resolve terrestrial water and energy budgets and a terrain- and channel-routing module and a conceptual subsurface flow bucket model to resolve streamflow. WRF-Hydro is designed for simulation, analysis, and prediction of surface and subsurface hydrologic and energy fluxes, with particular emphasis on the prediction of water exchanges to and from the atmosphere, across heterogeneous landscapes, and through stream and river networks and shallow groundwater aquifers. The WRF-Hydro system has served as the leading national hydrologic forecasting system for the U.S. National Weather Service (i.e. the NOAA National Water Model; Cosgrove et al., 2024) as well as in Romania, Israel, and the United Arab Emirates. Over the past two years (Water Years 2022 and 2023), the WRF-Hydro system has been implemented to provide seasonal water supply forecasts for multiple river basins in the Sierra Nevada region of California and Nevada assimilating real-time weather information, climate forecast data, and airborne lidar retrieved estimates of mountain snowpack from the Airborne Snow Observatory, Inc (ASO).

WRF-Hydro simulations were run with a multi-grid structure where soils and land cover/land use are prescribed at a 1-km spatial resolution and the model was forced with eight surface meteorological variables (precipitation, surface air temperature, east-to-west and north-to-south wind speed, long- and short-wave radiation, surface air pressure, and specific humidity) from the 1-km hourly observation-constrained Analysis of Record for Calibration (AORC; Fall et al., 2023) dataset that is used to drive the NOAA National Water Model (NWM). Model topography was based on the 1 arc-second National Elevation Dataset used by the National Water Model (NWM). Terrain routing processes controlling runoff and lateral exchanges of overland flow and subsurface saturated flow were represented on a 250 m model grid. Vegetation classifications were based on 30 m data from the 2016 National Land Cover Database (NLCD) (i.e., pre-fire classifications) and associated monthly leaf area index (LAI) and peak annual green vegetation fraction (GVF) were based on MODIS observed climatology from 2000-2008 which is consistent with the NWM configuration. Physics options and land surface parameters were selected to be consistent with the NWMv2.1 configuration. All simulations began on Oct. 1, 1999, and were initialized with a 14-year spin-up loop generated by the *baseline* simulation (Table 1) from Oct. 1, 1999 - Sept. 30, 2013. We did not calibrate the model for the purpose of this study, but the NWMv2.1 model configuration which was adopted for this study used the ICR gauge as a point of calibration during the 2009-2013 water years.

WRF-Hydro experiments incrementally introduced fire-related perturbations in a series of simulations and used a *baseline* simulation with no fire perturbations for comparisons to quantify the impact of compounding perturbations. Fire-perturbation simulations, summarized in Table 1, incrementally applied perturbations to (i) hydrological soil and surface water routing parameters (Section 2.2.1), (ii) vegetation area (Section 2.2.2), (iii) land cover classifications (Section 2.2.2), and (iv) snow albedo (Section 2.2.3). The simulation accounting for all fire-related perturbations considered herein (*Mod-params+GVF+Veg-class+Snow-alb*) applies a large range of land cover disturbances to the model configuration; however, fire can have important impacts through other perturbations to the land surface that are not considered in this study (Veraverbeke et al., 2012; French et al., 2016).

We ran a series of simulations from water years 2000-2022 (Table 1) to evaluate individual and compounding impacts of fire-related perturbations on simulated land surface hydrology in the study domain across a range of historically observed meteorological conditions. Although the study fire events only impacted hydrology in the post-fire 2018-

2022 water years, we imposed fire perturbations across the full historical period to evaluate the impacts of fire-related perturbations in WRF-Hydro simulations under the historically observed metrological conditions, considering potential fire impacts on the Feather River Basin water budget are likely to be sensitive to meteorological conditions. We evaluated model outputs from each water year as an ensemble member (interpreted as the model's response to fire perturbations under the unique meteorological conditions of respective water years), and the ensemble mean (i.e., multiyear average) was interpreted as the mean simulated land surface hydrological response to the climate conditions experienced in the study domain from 2000-2022.

Table 1. WRF-Hydro simulation experiment names and descriptions.

Experiment name	**Experiment description**
Baseline	"No-fire" simulation that does not account for fire impacts
Mod-params	Parameters associated with infiltration (REFKDT), surface roughness factor (OVROUGHRT), and surface retention depth factor (RETDEPRT) are adjusted based on burn severity classification (Section 2.2.1)
Mod-params+GVF	Simulation that modifies hydrologic soil and routing parameters and reduces greenness vegetation fraction (GVF) across burned areas (Sections 2.2.1; 2.2.2)
Mod-params+GVF+Veg-class	Simulation that modifies hydrologic soil and routing parameters, reduces GVF, and shifts vegetation classifications across burned areas (Sections 2.2.1; 2.2.2)
Mod-params+GVF+Veg-class+Snow-alb	Simulation that modifies hydrologic soil and routing parameters, reduces GVF, shifts vegetation classifications, and enhances snow albedo degradation rates across burned areas (Sections 2.2.1; 2.2.2; 2.2.3)

2.2.1 Accounting for fire disturbances on hydrologic and routing parameters

Fires directly impact hydrologic and routing parameters which LSMs rely on for accurate streamflow simulations (Verma & Jayakumar 2012). In this study we assumed fire impacts are generally proportional to fire severity and duration (Verma & Jayakumar 2012, Agbeshie et al. 2022). Therefore, we scale parameter adjustments by burn severity index (BSI) classifications (see Figure 1 for burn severity classification maps). BSI classification data used in this study are from the Monitoring Trends in Burn Severity (MTBS) dataset when available (Eidenshink et al., 2007) and the Burned Area Emergency Response (BAER) in instances when MTBS data was not available at the time of analysis (i.e., for post-2020 fires). These satellite-based burn-severity classification datasets record burn severity as unburned to very low-severity, low-severity, moderate-severity and high-severity. MTBS classifies burn severity using the differenced normalized burn ratio (dNBR), and BAER classifies soil burn severity using the burned area reflectance classification (BARC), noting there are known inconsistencies between BARC and fire effects on vegetation (Safford et al., 2008) which can introduce uncertainties in post-fire simulations. We recognize that post-fire changes in runoff generation can be highly site-specific (e.g., based on pre-fire vegetation type, soil type, slope, fire recurrence) and can change based on time since fire and weather conditions, but due to a lack of relevant observations to build these local relationships, in this study we tested a simple scaling scheme based on burn severity classifications alone that were generally consistent with previous research. We scaled the three fire-perturbed parameters, discussed below, by a factor of 0.5 for low-severity BSI, 0.3 for moderate-severity BSI, and 0.1 for high-severity BSI. For pixels that burned multiple times, these multiplication factors were first multiplied together before being applied to perturb respective parameters (e.g., if a pixel experienced a low-severity burn in one study fire event and a moderate-severity burn in a different study fire event then the corresponding multiplication applied to parameters was 0.5 x 0.3 = 0.15).

Ebel (2019) and Ebel and Moody (2020) suggested a field saturated conductivity adjustment of 0.30-0.37 from pre-fire to post-fire in the near-surface soil (top 1 cm), which is consistent with our moderate-burn severity modification of surface conductivity via the REFKDT scaling parameter used in the WRF-Hydro infiltration excess scheme (Schaake et al., 1996). Atchley et al. (2018) adjusted post-fire saturated hydraulic conductivity in the top 2-cm soil layer of Parflow-CLM by a factor of 0.04-0.14 for high-severity burn sites, which is consistent with our factor of 0.1 for the high-severity class. In Atchley et al. (2018) and

López-Vicente et al. (2020), post-fire overland roughness values were set to a bare soil value (0.011), which is slightly lower than our high-severity factor applied to the WRF-Hydro surface roughness parameter (OVROUGHRT) for a standard evergreen needleleaf forest type. Our moderate-severity overland roughness factor is generally consistent with a conversion from evergreen needleleaf forest to the grassland land cover type. We did not identify values to compare for changes due to fire to the WRF-Hydro maximum retention depth parameter (RETDEPRT) in previous literature, so our scaling factors were set to match the other parameter factors. Overall, this approach resulted in parameter adjustments across all burned classes, with higher severities yielding lower infiltration, smaller potential surface storage, and faster overland flowrate.

The primary goal of applying these parameter perturbations is to better understand whether WRF-Hydro simulations are notably impacted by perturbations in commensurate with fire disturbance magnitudes used in previous research. There is substantial uncertainty in the fire-perturbations we applied to the REFKDT, OVROUGHRT, and RETDEPRT parameters due to the large uncertainty in spatially-distributed fire-impacts on these parameters at the catchment scale and lack of local observations of these impacts. Therefore, the results discussed in this paper pertaining to these perturbations should be interpreted in the context of these known uncertainties, rather than interpreting these perturbations as an accurate representation of post-fire soil and routing parameters.

2.2.2 Accounting for fire disturbances on vegetation

Experiments designed to account for fire impacts on vegetation updated vegetation area and land cover classification model inputs across burned pixels. Vegetation area updates were informed by pre- to post-fire changes in satellite-monitored Fraction of Photosynthetically Active Radiation (FPAR) from the MODIS satellite (MOD15A2; Myneni et al., 2015). This study assumed MODIS observed changes to FPAR from pre- to post-fire periods are consistent with green vegetation fraction (GVF) changes. This assumption is consistent with the widely used WRF Preprocessing System (WPS) which is frequently used to derive Noah-MP LSM inputs (Lu et al., 2021); although using FPAR as a proxy for vegetation fraction in LSM simulations can introduce uncertainties (Filipponi et al., 2018; Myneni and Williams, 1994). MODIS observed distinct decreases to FPAR following each study fire event within respective fire perimeters (Figure 2). WRF-Hydro simulations employed the Noah-MP dynamic vegetation option 4, which assumes a constant vegetation area based on the peak GVF for respective pixels (He et al., 2023). To account for fire-

induced reductions to GVF, we imposed the MODIS-observed fractional change to peak annual GVF on the model input using eq. 1:

$$GVF_{post-fire,i} = GVF_{baseline,i} + GVF_{baseline,i} \times \frac{Obs_{post-fire,i} - Obs_{pre-fire,i}}{Obs_{pre-fire,i}} \quad \text{(Eq. 1)}$$

where $GVF_{post-fire,i}$ is used in fire-related perturbation experiments to reflect the fire impacted GVF for pixel i, $GVF_{baseline,i}$ is the baseline GVF for pixel i assuming no fire disturbance, $Obs_{pre-fire,i}$ is the multi-year median of MODIS-observed peak annual GVF for pixel i across all pre-fire years, and $Obs_{post-fire,i}$ is the multi-year maximum of MODIS-observed peak annual GVF for pixel i across all post-fire years. $GVF_{post-fire,i}$ was constrained to not exceed $GVF_{baseline,i}$ to assume that burned pixels do not have increased vegetated area. This constraint was applied to 8% of pixels in fire perimeters, whereas the other 92% of pixels in fire perimeters showed lower $GVF_{post-fire}$ relative to $GVF_{baseline}$.

For land cover classification shifts: pixels that experienced low-severity burning were maintained as original baseline land cover classifications, pixels with moderate-severity burning were updated to the grassland land cover classification, and pixels that experienced high-severity burning were updated to the barren or sparsely vegetated classification. Shifts to land cover classifications implicitly impact model parameters: leaf area index (LAI), height of the canopy, maximum rate of carboxylation at 25°C, and the overland flow roughness coefficient. These parameters were derived from the default Noah-MP parameter table which is publicly available: https://github.com/NCAR/wrf_hydro_nwm_public. These assumed fire-induced land cover classification shifts are less aggressive than previous modeling analyses that account for fire impacts on hydrology, which imposed homogenous shifts to the barren or sparsely vegetated classification over entire burn scars (Maina and Siirila-Woodburn, 2020; Li et al., 2023). The land cover updates applied herein are designed to roughly represent fire-induced land cover shifts because post-fire observed land cover classifications (e.g., from the MODIS MCD12 products) were not available at the time of experimentation. This source of LSM and hydrologic model uncertainty motivates up-to-date monitoring and publishing of land cover classification and vegetation data that can inform operational hydrologic modeling systems over burned areas.

2.2.3 Accounting for fire-enhanced snow albedo degradation

Snow albedo tends to degrade faster following fires due to soot and burned debris shedding from standing trees onto the snowpack which darkens the snow resulting in reduced

albedo (Gleason et al., 2013, 2019; Gleason and Nolin, 2016). Additionally, less shading results in more solar radiation being absorbed by the snowpack which also favours faster snow albedo degradation (Harpold et al., 2014). Fire-enhanced snow albedo degradation, which was accounted for in the most comprehensive WRF-Hydro experiment (*Mod-params+GVF+Veg-class+Snow-alb*), was designed to allow the model simulated albedo to degrade to the mean observed snow albedo from a late spring ASO snow survey within the Dixie Fire burn scar (Painter et al., 2016). Specifically, a spring post-fire ASO fly over in the Feather River Basin (March 31 – April 2, 2022) observed substantially lower snow albedo over burn scars (mean and standard deviation = 0.40 and 0.15) relative to measurements over unburned areas (mean and standard deviation = 0.79 and 0.14), resulting in large systematically positive snow albedo biases in the *baseline* WRF-Hydro simulation within burn scars (Figure 3; mean [standard deviation] of baseline snow albedo bias = 0.45 [0.15]). We chose to inform the fire-aware snow albedo parameter updates using this late-season ASO survey because it was difficult to inform snow albedo parameter updates using earlier surveys in February and March which were more significantly impacted by fresh snowfall, and thus had more noise regarding fire-enhanced snow albedo degradation. The mean and standard deviation for observed visible snow albedo from the four Feather River Basin ASO surveys in 2022 over burned and no-burn areas are recorded in Table S1. We account for fire-enhanced snow albedo degradation by implementing a code update into the WRF-Hydro model that adjusted parameters controlling the visible snow albedo degradation rate in the BATS ground snow albedo scheme (https://github.com/RAbolafiaRosenzweig/WRF-Hydro-BATS_fire_enhanced_snow_albedo_degradation), which is the most sophisticated snow albedo physics option in the open-source Noah-MP LSM that computes ground snow albedo for direct and diffuse radiation in visible and NIR bands (Yang et al., 1997).

BATS computes broadband ground snow albedo (α_s) as the average of visible ($\alpha_{V,s}$; λ < 0.7 μm) and NIR ($\alpha_{NIR,s}$; $\lambda \geq 0.7$ μm) snow albedo:

$$\alpha_s = 0.5(\alpha_{V,s} + \alpha_{NIR,s}) \qquad \text{(Eq. 2)}$$

where,

$$\alpha_{V,s} = W_{direct}\alpha_{V,s-direct} + W_{diffuse}\alpha_{V,s-diffuse} \quad \text{(Eq. 3)}$$

$$\alpha_{NIR,s} = W_{direct}\alpha_{NIR,s-direct} + W_{diffuse}\alpha_{NIR,s-diffuse} \quad \text{(Eq. 4)}$$

W_{direct} and $W_{diffuse}$ are the fractions of total transmitted solar radiation that is direct and diffuse, respectively. Direct visible ($\alpha_{V,s-direct}$) and NIR ($\alpha_{NIR,s-direct}$) snow albedos are solved as:

$$\alpha_{V,s-direct} = \alpha_{V,s-diffuse} + V_{DIR} f_{Z,s}(1 - \alpha_{V,s-diffuse}) \quad \text{(Eq. 5)}$$

$$\alpha_{NIR,s-direct} = \alpha_{NIR,s-diffuse} + NIR_{DIR} f_{Z,s}(1 - \alpha_{NIR,s-diffuse}) \quad \text{(Eq. 6)}$$

$\alpha_{V,s-diffuse}$ and $\alpha_{NIR,s-diffuse}$ are diffuse visible and NIR albedo, respectively. V_{DIR} and NIR_{DIR} are the *cosZ* factor for direct visible and NIR snow albedo, respectively. $f_{Z,s}$ is a factor, ranging between 0 and 1, to parameterize the effect of solar zenith angle on snow albedo. Diffuse albedos are calculated as:

$$\alpha_{V,s-diffuse} = \alpha_{V,new}(1 - V_{age} f_{age}) \quad \text{(Eq. 7)}$$

$$\alpha_{NIR,s-diffuse} = \alpha_{NIR,new}(1 - NIR_{age} f_{age}) \quad \text{(Eq. 8)}$$

where $\alpha_{V,new}$ and $\alpha_{NIR,new}$ are fresh-snow visible and NIR albedo with solar zenith angle less than 60°. f_{age}, ranging between 0-1, is a snow-age factor designed to account for the effects of snow grain growth from vapor diffusion, additional effects of snow grain growth near or at the freezing of meltwater, and snow impurification from dirt and soot (i.e., set equal to the dirt-soot parameter in the Noah-MP parameter table). Details on f_{age} calculations are provided in Abolafia-Rosenzweig et al. (2022b).

Sensitive snow albedo parameters that were adjusted were informed by a previous Noah-MP BATS snow albedo sensitivity analysis (Abolafia-Rosenzweig et al., 2022b). Pixels which experienced high-severity burning increased the *dirt-soot* and V_{age} parameters to 0.6 and 0.9 allowing snow albedo to degrade to 0.4 during a 20-day snow free period, which is equal to the mean burn scar snow albedo observed by the ASO measurements (Figure 3). Pixels which experienced moderate-severity burning adjusted *dirt-soot* and V_{age} to 0.5 and 0.67 which resulted in snow albedo degradation to 0.57 in a 20-day snow free period. Pixels which experienced low-severity burning adjusted *dirt-soot* and V_{age} to 0.4 and 0.43 which resulted in snow albedo degradation to 0.71 in a 20-day snow free period. Pixels that were not burned in the study fires used default *dirt-soot* and V_{age} values (0.3 and 0.2, respectively) resulting in relatively slower snow albedo degradation over no-burn areas: reducing to 0.84 over a 20-day snow free. Parameter adjustments for moderate- and low-severity burning are calculated using linear interpolation between the adjustment for the high-severity and the *baseline* parameters which assumes snow albedo degradation increases with increasing burn severity; however, this assumption and corresponding linear interpolation are largely uncertain and requires in-depth quantifications of the influence of burn-severity on surface snow albedo degradation that is out of the scope of this modeling-focused study.

These snow albedo parameter adjustments have substantial uncertainty and are primarily implemented to roughly reflect the impact of fire-enhanced snow albedo

degradation in burned areas. For instance, relationships between burn severity and albedo degradation vary as a function of vegetation type in nature because severely burned grasslands will not shed soot and burned debris on post-fire snowpack as observed in burned forests. Furthermore, the average snow albedo within burn scars from a single ASO flyover does not provide a robust presentation of spatiotemporal impacts of fire on snow albedo. Due to the uncertainty related to this snow albedo parameterization, we implement the fire-aware snow albedo parameterization in WRF-Hydro to roughly account for fire-enhanced snow albedo degradation in a manner that allows the model to simulate degraded snow albedo to be consistent with a snapshot of spatially averaged ASO monitored snow albedo. This representation likely does not adequately simulate true spatiotemporal variability of snow albedo in burn scars nor is it likely to accurately simulate the true corresponding hydrologic impacts so we encourage future research to evaluate pathways for more sophisticated post-fire snow albedo degradation model updates (e.g., Gleason and Nolin, 2016) that can be implemented in operational modeling systems.

2.3 WRF-Hydro streamflow validation

Validation of pre- and post-fire simulations compared simulated and in-situ observed Q anomalies at a daily timestep. This validation first quantified the accuracy of *baseline* Q anomalies during pre-fire periods to establish a baseline performance in which post-fire changes in skill were compared with. Post-fire validations compared skill from the *baseline* and the most comprehensive fire-adjusted simulation (i.e., *Mod-params+GVF+Veg-class+Snow-alb*) to determine whether accounting for fire perturbations in the model reduces post-fire model biases and uncertainties.

Prior to comparing modelled and observed Q, we converted respective timeseries to standardized anomalies using eq. 2:

$$Q_{anomaly,t} = \frac{Q_t - \bar{Q}_{prefire}}{\sigma_{Q-prefire}} \qquad \text{(Eq. 9)}$$

where Q_t is Q from day t, $\overline{\mathrm{Q}}_{prefire}$ is the pre-fire time series mean, and $\sigma_{Q-prefire}$ is the pre-fire time series standard deviation. Because Q time series are not normally distributed, the anomaly conversion was exclusively used to remove pre-fire biases between simulated and observed time series (mean and variance), rather than interpretation of anomaly magnitude in a z-score context (Williams et al., 2022; Abolafia-Rosenzweig et al., 2024b). It is important to remove background systematic biases to allow isolation of fire-induced discrepancies

rather than analysing results confounded by systematic biases between simulations and observations that are not related to fire-disturbances. This standardized approach limits the meaning of bias and NSE, and thus bias and NSE skill scores reported in this paper should primarily be used in the context of comparisons between fire-aware and no-fire simulations and for skill score shifts from pre- to post-fire periods.

Statistical differences in biases between the *baseline* and fire-aware simulations were computed with the widely used 2-tailed Wilcoxon rank sum test. Statistical differences in R^2 and NSE were computed with permutation testing. Permutation tests are based on resampling the original data without replacement to test the hypothesis of no statistical difference between skill scores calculated from different simulations. This is performed by: (i) calculating the absolute difference between skill scores, (ii) pooling data from comparison datasets together, (iii) shuffling the data randomly and calculating differences in skill scores between random samples equivalent to the length of the original samples, (iv) repeating step (iii) 10,000 times, and (v) calculating the proportion of shuffled absolute differences in skill scores that exceed the originally calculated skill score differences when data was organized.

Pre-fire validation periods were selected to begin either at the start of the 2000 water year or at the start of the in-situ record (if observations were not available starting at Oct. 1, 1999) and span until the end of the month prior to the ignition of the first study fire event in respective catchments. Post-fire periods were selected as periods starting on the first of the month after the containment of the latest study fire event in respective catchments and range until the end of the study period (Sept 30, 2022). Post-fire evaluations are limited because they are relatively short (11-12 months) and dry (negative observed mean streamflow anomalies). Thus, the post-fire model validations did not consider wet regimes or allow consideration of uncertainties related to vegetation regrowth. Pre- and post-fire period selections only considered the five major fire events shown in Figure 1, but due to burning in the study domain excluding these major fire events (Figure S1) the pre- to post-fire model skill comparisons may be confounded by the fact that there is no true pre-fire period with negligible burning. However, comparisons between these periods are still valid and useful to determine the impacts of these relatively major fire events on model skill. Pre-fire periods for MFF, NFF and EBNFF were selected as: 10/1999-07/2020, 12/2004-06/2021, and 06/2007-08/2019, respectively, with varying start dates based on observation data availability. Post-fire periods for MFF, NFF and EBNFF were selected as: 11/2021-09/22, 10/2021-09/2022, and 10/2021-09/2022, respectively.

We reported widely used metrics from previous hydrologic model evaluations to quantify model skill in this study: mean anomaly bias, the coefficient of determination (R^2) and the Nash Sutcliffe efficiency (NSE) (Moriasi et al., 2007, 2015). Skill categorizations are based on Moriasi et al. (2015): $R^2>0.85$, $0.70\leq R^2\leq 0.85$, $0.50<R^2<0.70$ and $R^2\leq 0.50$ are considered very good, good, satisfactory and not satisfactory performance, respectively, and NSE>0.80, 0.70≤NSE≤0.80, 0.50<NSE<0.70 and NSE≤0.50 are considered very good, good, satisfactory and not satisfactory performance, respectively.

2.4 Water budget sensitivities to fire disturbances

We evaluated the response of the WRF-Hydro simulations to fire-related perturbations by quantifying differences between fire-adjusted and *baseline* simulations (Table 1) for land surface water budget components: Q (i.e., routed surface flow + routed subsurface flow), subsurface flow, ET and its partitions (transpiration (E_{tran}), evaporation of canopy-intercepted water (E_{can}), and bare ground evaporation plus sublimation (E_{dir})), snow water equivalent (SWE), and soil moisture (SM). Catchment-scale Q impacts were evaluated at CADWR gauge locations (Figure 1), whereas other components were evaluated at the catchment scale using spatial averaging. Snow ablation rates were calculated following the methodology presented in Xiao et al. (2021), as the rate of change in SWE between 80% to 20% of peak SWE during the falling limb of the annual SWE cycle. Simulated day of snow disappearance (DSD) was defined as the first day when SWE=0 after peak SWE for respective water years at respective model pixels.

3. RESULTS

3.1 WRF-Hydro streamflow validation

In the three study catchments the *baseline* simulation had good to very good pre-fire skill simulating daily (R^2 = 0.72-0.87; NSE =0.70-0.87) and monthly (R^2 = 0.79-0.93; NSE =0.78-0.93) streamflow anomalies at each study catchment (Moriasi et al., 2015) (Figure 4a,c,e; Figure S2a,c,e). In post-fire periods, skill from the *baseline* simulation only provided satisfactory performance at the MFF catchment for R^2 (R^2=0.61) but unsatisfactory performance for R^2 at NFF and EBNFF (R^2<0.5) and unsatisfactory NSE across all three study catchments (NSE<0.5) for daily comparisons (Moriasi et al., 2015) (Figure 4b,d,f). The *baseline* simulation also simulated consistently negative post-fire biases for streamflow

anomalies (Figure 4; Figure S2) and had consistently degraded skill in monthly comparisons as well (R^2=0.00-0.66; NSE = -1.56-0.61). Accounting for fire-related perturbations in the *Mod-params+GVF+Veg-class+Snow-alb* simulation significantly (p<0.001) reduced post-fire daily Q anomaly biases at each catchment (by 0.03 to 0.15) and significantly (p<0.001) increased post-fire model R^2 and NSE to a satisfactory 0.63 and 0.60 at the NFF catchment, relative to the *baseline* simulation (Figure 4b,d,f). Likewise, monthly comparisons also showed improved post-fire streamflow biases in the *Mod-params+GVF+Veg-class+Snow-alb* simulation relative to the *baseline* simulation (Figure S2b,d,f). To further evaluate whether the imposed fire perturbations allow model simulations to be more physically consistent with post-fire terrestrial hydrology, we evaluated whether the fire-aware simulation has lower skill in simulating pre-fire streamflow than the *baseline* simulation. Figure S5 shows that the *Mod-params+GVF+Veg-class+Snow-alb* consistently had lower skill than *baseline* simulated Q in pre-fire years; however, only differences in NSE from *baseline* and *Mod-params+GVF+Veg-class+Snow-alb* simulations at the NFF and EBNFF catchments were statistically significant (p<0.01). Overall, consistently reduced post-fire anomaly underestimates from the fire-aware simulation may indicate that the imposed fire-related perturbations can improve the model's ability to simulate fire-enhanced streamflow; however, instances of similar skill scores between *Mod-params+GVF+Veg-class+Snow-alb* and *baseline* in pre- and post-fire periods indicate that the fire-treatments considered herein likely do not adequately resolve fire-related model uncertainties and more sophisticated observationally-constrained parameterizations of soil properties, snow albedo, and vegetation classifications should be considered in future model developments.

At the MFF catchment, a key discrepancy between simulated and observed post-fire Q-anomalies occurred during the snow accumulation period (Dec. 2021 – Jan. 2022) when observations showed substantially larger streamflow anomalies relative to the *Mod-params+GVF+Veg-class+Snow-alb* and *baseline* simulations (Figure S3a). During this period, both observed and simulated spikes in Q-anomalies responded to precipitation events, with observed anomalies responding with higher sensitivity. These discrepancies in Q-anomaly spikes may be attributable to combinations of uncertainties in: (i) rain/snowfall magnitude and partitioning, (ii) rain-on-snow runoff and melt responses, and (iii) post-fire soil infiltration alterations. The most obvious discrepancies between simulated and observed Q-anomalies occurred in the EBNFF catchment where observations had more acute streamflow responses to precipitation events than model simulations (Figure S3c). For example, in late-October, observations showed a large spike in Q-anomalies in response to a

precipitation event, whereas simulations showed a minor and slow response in Q-anomalies while simulating increases in soil moisture and SWE. This indicates that in the model, the precipitation largely contributes to SWE and soil moisture instead of Q (as observed). This is consistent with potential uncertainties in rain-snow partitioning, soil moisture, and post-fire soil infiltration alterations. Throughout the EBNFF snow accumulation period, observed Q-anomalies had acute responses to precipitation events whereas the model fails to simulate these streamflow spikes. This further supports that the post-fire uncertainties are partially attributable to uncertainties in meteorological forcing (e.g., incorrect rain/snow partitioning) or uncertain rain-on-snow runoff and melt responses. Accounting for fire perturbations provided the largest improvement at the NFF catchment (Figure 4d). The largest post-fire Q-anomaly error for the *baseline* simulation at NFF was in response to a late-October precipitation event when observations show a large spike in Q-anomalies up to 5.0, whereas the corresponding *baseline* simulated Q-anomaly spike only reached 1.2 (Figure S3b). Accounting for fire-impacts in the *Mod-params+GVF+Veg-class+Snow-alb* simulation allowed the model to better capture this Q-anomaly spike, reaching 5.5. More minor discrepancies between *baseline* and *Mod-params+GVF+Veg-class+Snow-alb* simulated Q occurred in the spring when the fire-aware simulation melted snow at a faster rate and simulated higher streamflow. However, observed Q-anomalies did not show the signal of fire-enhanced spring ablation and streamflow, but it is difficult to determine whether this is due to lack of fire impacts on snow and Q in nature, or whether the observations may be impacted by other unmodeled factors such as human diversions of surface water.

Comparing multidecadal pre-fire periods to relatively short and dry post-fire periods is useful to provide historical context of post-fire skill. However, further evaluations are required to determine whether relatively lower skill in post-fire periods was likely to have been induced by fire-related uncertainties. Previous research has established that LSMs have difficulty simulating water-limited ET reductions (Ukkola et al., 2016; Mu et al., 2021; Li et al., 2021) so we consider whether the degraded model performance in post-fire years shown in Figure 4 is attributable to a small post-fire data record during a relatively dry and water-limited period (mean post-fire observed Q-anomalies = -0.16 to -0.14 varying by catchments) with observed peak Q anomalies that ranged from 1.98-4.95. Figure S4 shows pre-fire model evaluations from the *baseline* simulation only considering dry pre-fire periods comparable to respective post-fire periods: same start month and number of days with valid observations as corresponding post-fire periods with a negative mean daily observed Q-anomaly and similar

peak flow (see Figure S4 for further details). The *baseline* simulation has higher skill in two out of three of the hydrologically similar pre-fire periods relative to *baseline* post-fire skill at the MFF catchment. The one "pre-fire" period at MFF (Nov. 1, 2009 – Sept. 30, 2010) when the *baseline* simulation had lower skill than the corresponding post-fire period followed nearly 40,000 acres of burning in 2008 (Figure S1) which may confound the pre- to post-fire skill comparison because the pre-fire skill can be impacted by fires other than the five study fire events. The *baseline* skill during hydrologically similar pre-fire periods was consistently better than corresponding post-fire skill at the NFF and EBNFF catchments, particularly for NSE and bias. For instance, post-fire Q-anomaly underestimates (biases = -0.16 - -0.21) largely exceeded the pre-fire bias magnitudes during comparable periods (biases = -0.03 – 0.10). Relatively better skill from the *baseline* simulation during hydrologically similar pre-fire periods, compared to post-fire *baseline* skill, further supports that a portion of the degraded pre- to post-fire model skill and bias changes in the *baseline* simulation are likely due to fire disturbances that are not accounted for in the *baseline* simulation.

3.2 Fire-related disturbance impacts to the terrestrial water budget

3.2.1 Impacts on streamflow and subsurface flow

The most comprehensive fire-aware experiment (*Mod-params+GVF+Veg-class+Snow-alb*) simulated enhanced annual Q by 6-115% (multiyear mean = 37%), 3-18% (multiyear mean =8%), and 4-28% (multiyear mean = 16%) at the EBNFF, MFF, and NFF catchments, respectively, relative to the *baseline* simulation (ranges are from temporal variability across 2000-2022 water years) (Figure 5; Figures S6-S9). There were minimal differences in simulated annual Q between the *Mod-params* and *baseline* experiments (multiyear-mean differences are <0.1% in each study catchment). Fire-induced reductions to GVF accounted for the majority of the fire-enhanced Q: differences in annual Q between the *Mod-params+GVF* and *baseline* experiments were 7-113% (multiyear mean = 38%), 3-18% (multiyear mean = 9%), and 5-27% (multiyear mean = 16%) at EBNFF, MFF, and NFF catchments, respectively (Figure 5; Figures S6-S9). After accounting for GVF reductions, altering vegetation classifications only has a relatively minor impact on annual catchment discharge, with minor differences in annual Q between *Mod-params+GVF+Veg-class* and *Mod-params+GVF* simulations (multiyear mean difference of <0.2% across each study catchment). Enhancing snow albedo degradation rates in burned areas did not notably alter annual Q compared to simulations that did not consider fire-impacts on snow albedo:

multiyear mean differences between *Mod-params+GVF+Veg-class+Snow-alb* and *Mod-params+GVF+Veg-class* annual Q were <1% at each study catchment.

At the daily timescale, there were typically minimal differences in Q between the *Mod-params* and *baseline* experiments; however, modified parameters favoured substantially enhanced streamflow during some precipitation events with differences in daily Q between the *Mod-params* and *baseline* experiments exceeding 10% of mean daily *baseline* Q during 8 days, 64 days, and 24 days in the 23-year simulations at the EBNFF, MFF, and NFF catchments, with peak changes in daily Q reaching 695-1032 cfs (Figures S7-S9). Mean differences between daily Q from *Mod-params+GVF* and *baseline* experiments were substantial: 25% (164 cfs), 7% (113 cfs), and 14% (484 cfs) at the EBNFF, MFF, and NFF catchments, respectively. Imposing fire-related vegetation classification shifts resulted in minor differences between *Mod-params+GVF+Veg-class* and *Mod-params+GVF* at the daily timescale; namely, enhanced Q from *Mod-params+GVF+Veg-class* from January through March (by 1-2% across catchments) and relatively lower Q from *Mod-params+GVF+Veg-class* from May through June by 1-4% across catchments. These differences are physically consistent with landcover classification shifts favoring enhanced ablation and reduced SWE (Section 3.2.3). Enhancing snow albedo degradation rates in burned areas enhanced Q from January through March (by 2-5% across catchments) and reduced Q from April through June (by 2-8% across catchments), based on differences between *Mod-params+GVF+Veg-class+Snow-alb* and *Mod-params GVF+Veg-class* simulations. These streamflow differences are physically consistent with enhanced snow ablation during accumulation and ablation seasons from simulations that perturbed snow albedo parameters in burned areas (Section 3.2.3). Overall, the cumulative impacts of fire on Q accounted for in the *Mod-params+GVF+Veg-class+Snow-alb*, relative to *baseline*, favoured persistently enhanced daily Q; however, *Mod-params+GVF+Veg-class+Snow-alb* tended to simulate minor reductions in late spring to early summer Q (varying by catchment) due to earlier snow disappearance relative to the *baseline* simulation (Figures 5; Figure S7-S9).

Mod-params+GVF+Veg-class+Snow-alb simulated enhanced daily subsurface flow (by 72-116% across catchments) relative to the *baseline* simulation; however, faster snow depletion in the fire-aware simulation resulted in notable subsurface flow reductions from mid-April through mid-June due to accelerated snow disappearance (Figure 6; Figure 10). *Mod-params* simulated slightly reduced daily subsurface flow relative to *baseline* (mean catchment reductions <1% across catchments), indicating modelled subsurface flow is

relatively insensitive to the hydrologic parameter modifications imposed in this study (Figure 6). *Mod-params+GVF* simulated substantially greater subsurface flow than *baseline* by 114%, 70%, and 116% at EBNFF, MFF and NFF catchments, respectively. Accounting for fire-related vegetation classification shifts in *Mod-params+GVF+Veg-class* did not substantially impact annual subsurface flow relative to *Mod-params+GVF*, with <1% reductions across each catchment for the total water year, a 2% increase from January through March and then a 4% reduction from April through June. These subsurface flow differences are physically consistent with *Mod-params+GVF+Veg-class* simulating enhanced snow ablation relative to the *Mod-params+GVF* simulation (Section 3.2.3). *Mod-params+GVF+Veg-class+Snow-alb* simulated enhanced subsurface flow relative to *Mod-params+GVF+Veg-class* throughout the water year until early- to mid-April when accelerated snow depletion from enhanced snow albedo degradation caused earlier snow disappearance and in turn reduced subsurface flow.

3.2.2 Impacts on evapotranspiration

The *Mod-params+GVF+Veg-class+Snow-alb* experiment simulated reduced annual ET by 17-31% (multiyear mean = 22%), 11-23% (multiyear mean =15%), and 20-36% (multiyear mean = 26%) at EBNFF, MFF, and NFF catchments, respectively, relative to the *baseline* simulation (ranges from temporal variability) (Figure 7). There were minimal differences in annual ET between the *Mod-params* and *baseline* simulations (multiyear-mean differences are <0.1% at each study catchment). Fire-induced reductions to GVF accounted for the bulk of ET reductions (Figure 7). Minor differences between ET from *Mod-params+GVF+Veg-class* and *Mod-params+GVF* experiments were predominately caused by enhanced E_{dir} in the *Mod-params+GVF+Veg-class* simulation which partially countered the fire-induced ET reductions (Figure S10). Imposing enhanced snow albedo degradation within burned areas in *Mod-params+GVF+Veg-class+Snow-alb* slightly altered ET timing relative to the *Mod-params+GVF+Veg-class* simulation. Namely, enhanced snow albedo degradation caused enhanced solar radiation absorbed by the snowpack which increased sublimation in snow covered areas and decreased soil evaporation in warm months (e.g., May through August) due to earlier snow disappearance (Figure 7; Figure S11).

Mod-params+GVF+Veg-class+Snow-alb simulated ET reductions across 91-100% of burned pixels in fall, winter, and summer, relative to *baseline* (Figure 8). In spring, when fire-related E_{dir} enhancements peaked (Figure 9), there was spatial heterogeneity in ET differences with 34% of burned areas showing enhanced ET from the *Mod-*

params+GVF+Veg-class+Snow-alb experiment, relative to the *baseline* simulation (Figure 8g). One-hundred percent of the burned pixels with fire-enhanced spring ET had enhanced E_{dir} with a robust Pearson correlation between increased spring E_{dir} and increased spring ET (r=0.82, p<0.01), supporting a strong control on spring ET from E_{dir}. There was a transition period in mid-May when fire-related reductions to E_{tran} tended to outweigh enhanced E_{dir}, followed by fire-related ET and E_{tran} reductions peaking in summer (Figures 7-9).

3.2.3 Impacts on snowpack

Mod-params+GVF+Veg-class+Snow-alb simulated heterogeneous directional changes to peak SWE relative to the *baseline* simulation: mean catchment peak SWE differences ranging from -4% to 0.3% (Figure 10) and the burned pixel peak SWE difference interquartile range (IQR) was -3 to 8%. These heterogeneous impacts were largely attributable to heterogeneity in vegetation classification and snow albedo parameter alterations and the competing impacts of perturbations. Namely, *Mod-params+GVF* simulated increased peak SWE in 95% of instances (catchment mean peak SWE increase = 8-14%), relative to *baseline*, indicating that reducing vegetation area generally favoured greater snow accumulation. *Mod-params+GVF+Veg-class* simulated peak SWE decreases in 19% of instances relative to *baseline*, with 95% of these instances having a high burn severity and *baseline* classifications of evergreen needleleaf or mixed forest. Conversely, only 12% of the pixels that showed increased peak SWE from the *Mod-params+GVF+Veg-class* experiment had *baseline* classifications of evergreen or mixed forest and experienced a high burn severity. This indicates that imposing conversions from forested to barren or sparsely vegetated classifications for the high-burn severity class was a key contributor to heterogeneous fire-related impacts on peak SWE. *Mod-params+GVF+Veg-class+Snow-alb* simulated decreased peak SWE in 36% of instances, with a higher tendency for peak SWE decreases at moderate and high-severity burned pixels (48-50%) relative to low-burn severity pixels (11%). Thus, the burn-severity dependent treatment of snow albedo parameter perturbations, which tended to counter enhanced SWE from GVF reductions, also contributed to heterogeneous fire-related impacts on SWE.

The *Mod-params+GVF+Veg-class+Snow-alb* simulation consistently modelled earlier snow disappearance relative to the *baseline* simulation: mean, [IQR] DSD difference = -8, [-13 to -1 days]. *Mod-params+GVF+Veg-class+Snow-alb* simulated higher winter and spring SWE in multiyear averages at 54% and 40% of burned pixels, relative to *baseline* (Figure 11). Fire-related perturbations causing a transition from slightly enhanced winter

SWE to reduced spring and summer SWE is also shown in the catchment scale multiyear-averaged timeseries. This transition reflects the competing impacts of fire-related perturbations favoring enhanced ground snow accumulation due to reduced canopy interception and enhanced ablation due to greater solar radiation being absorbed by the snowpack in response to vegetation reductions and snow albedo degradation (Figure 10). GVF reductions tended to enhance melt season snow ablation rates (by 0.15 – 0.38 mm/day across catchments). This was caused by relatively more incoming solar radiation being partitioned to latent heat flux to melt and sublimate the snowpack and less solar radiation partitioned to sensible heat flux to increase the vegetation temperature because a relatively larger portion of a model pixel was categorized as ground-snow-covered rather than vegetated after reducing GVF. Competing impacts of GVF reductions on snow, favoring greater peak SWE and faster ablation, ultimately results in the *Mod-params+GVF* tending to simulate a later day of snow disappearance (DSD) (mean, [IQR] DSD difference = 2.8, [-1 to 6] days across burned pixels) relative to *baseline*. Thus, the impact of GVF reductions on increased snow accumulation tended to outweigh the impact of accelerated snow ablation when considering DSD. Fire-related landcover classification shifts in the *Mod-params+GVF+Veg-class* simulation enhanced ablation, resulting in reduced peak SWE (catchment average peak SWE reductions = 3-5%) and a tendency for earlier snow disappearance (mean, [IQR] DSD difference = -2.9 days, [-4 to 0 days]), relative to the *Mod-params+GVF* simulation. Imposing fire-related acceleration of snow albedo degradation in the *Mod-params+GVF+Veg-class+Snow-alb* simulation further enhanced snow ablation, favouring reduced peak SWE (catchment average peak SWE reductions = 6-11%) and earlier snow disappearance (mean, [IQR] DSD difference = -7.7 days, [-11 to -2 days]) relative to the *Mod-params+GVF+Veg-class* simulation.

3.2.4 Impacts on soil moisture

The *Mod-params+GVF+Veg-class+Snow-alb* experiment simulated a 4-9% soil moisture increase in the multiyear mean daily catchment comparisons, relative to the *baseline* simulation (Figure 12). Fire-related perturbations enhanced soil wetness in the falls when >99% of burned pixels had increased soil moisture, and 91% increased by at least 10% (Figure 13a,e). Fire-related perturbations enhanced soil wetness in winters when >99% of burned pixels had increased soil moisture, but only 36% increased by at least 10% (Figure 13b,f). Fire-related perturbations enhanced soil wetness in summers when >99% of burned pixels had increased soil moisture, and 48% increased by at least 10% (Figure 13d,h). Fire-

related perturbations had a lesser impact on soil wetness in springs when 73% of burned pixels had increased soil moisture and <1% increased by at least 10% (Figure 13c,g). Simulated soil moisture was not notably impacted by the hydrologic parameter adjustments made in this study, and simulated soil moisture was most impacted by the GVF reductions (Figure 12). Namely, the *Mod-params+GVF* experiment simulated 4-9% wetter soil moisture relative to the *baseline* simulation based on multiyear-average daily comparisons across the three catchments (Figure 12), with enhanced soil wetness being attributable to reduced ET (Sect. 3.2.2). The seasonality of enhanced soil wetting from GVF reductions (i.e., *Mod-params+GVF* minus *baseline*) is characterized as: enhanced wetting peaking in Fall (by 11-19%), then reduced soil wetting impacts in winter (by 2-9%), minor differences in spring (by 0.4-1.2%) and then wetter soil moisture in the summer (by 4-7%) (Figure 12). Accounting for fire-related changes to vegetation classifications and snow albedo generally resulted in minor adjustments to soil moisture relative to the *Mod-params+GVF* experiment. Differences in soil moisture between *Mod-params+GVF+Veg-class+Snow-alb* and *Mod-params+GVF* are characterized as slightly increased wetness when snow albedo darkening enhanced ablation from January through March and slightly increased dryness from April through June because *Mod-params+GVF+Veg-class+Snow-alb* simulated relatively faster snow depletion (Figures 10,12).

4. DISCUSSION

The WRF-Hydro *baseline* simulation had significant post-fire streamflow anomaly underestimates which is consistent with Abolafia-Rosenzweig et al. (2024b) who found pre- to post-fire bias shifts in the Noah-MP LSM. Post-fire bias reductions from the fire-aware *Mod-params+GVF+Veg-class+Snow-alb* simulation supports that fire-related model perturbations played a significant role in post-fire model accuracy. Despite lower biases during post-fire periods from this fire-aware simulation, there is still inadequate post-fire accuracy, emphasizing the continued need to focus on land surface and hydrological model accuracy and improvements in burned areas. Therefore, future improvements in post-fire LSM accuracy are required to provide reliably accurate depictions of fire impacts to the terrestrial water budget.

WRF-Hydro simulations were largely impacted by vegetation area reductions, with smaller impacts corresponding to adjustments made to the hydrologic soil and routing parameters, land cover classifications, and snow albedo parameters. Simulations that accounted for vegetation area reductions tended to simulate enhanced annual streamflow and

reduced annual ET due to transpiration reductions. These results are consistent with previous analyses which found fire disturbances favour enhanced streamflow (Williams et al., 2022; Abolafia-Rosenzweig et al., 2024b; Stoof et al., 2012), although these results are likely domain-specific with prior research finding fire-disturbances tend to favour suppressed streamflow in dry water-limited watersheds (Goeking and Tarboton, 2022). This analysis supports that fire-induced ET reductions exert greater control on soil moisture and subsurface flow than fire-induced changes to soil hydrophobicity in the WRF-Hydro modelling system, which result is consistent with previous research (Bart and Tague, 2017; Cardenas and Kanarek, 2014). However, it is difficult to determine whether the small model response to hydrologic and routing parameter perturbations shown herein are reasonable or potentially model scheme specific. Relatively larger model responses to GVF reductions shown in this study, compared to the previous research conducted by Abolafia-Rosenzweig et al. (2024b), are likely attributable to the dynamic vegetation option used in Noah-MP LSM simulations. Namely, this study imposed GVF reductions to the peak GVF using Noah-MP's dynamic vegetation option 4 (i.e., the default Noah-MP Dynamic Vegetation option), whereas Abolafia-Rosenzweig et al. (2024b) forced simulations with MODIS-observed GVF which inherently accounted for GVF reductions using dynamic vegetation option 7 (He et al., 2023).

5. CONCLUSIONS

This study incrementally imposed a suite of fire-related perturbations in WRF-Hydro simulations across the heavily burned Feather River Basin in northern California. These perturbations focused on fire-related changes to hydrologic soil and routing parameters, vegetation area, land cover classifications and associated vegetation properties, and snow albedo degradation. The most comprehensive fire-aware experiment (*Mod-params+GVF+Veg-class+Snow-alb*) consistently simulated enhanced annual streamflow, subsurface flow, and soil moisture, relative to the *baseline* simulation which did not account for fire impacts. Modelled streamflow enhancements from this fire-aware simulation occurred throughout the water year, excluding early-summer (e.g., May-June) when the *baseline* experiment simulated more snow melt because the fire-related perturbations tended to accelerate snow depletion. Enhanced annual streamflow and soil moisture in simulations that imposed fire-related perturbations were predominately attributable to vegetation area reductions which reduced transpiration. Vegetation area reductions also tended to enhance simulated ground snow accumulation due to less interception; however, vegetation reductions and snow albedo darkening also tended to enhance radiation absorbed by the snowpack and

corresponding increases to snow ablation. On average, this resulted in slightly reduced peak SWE and faster snow disappearance from the fire-aware *Mod-params+GVF+Veg-class+Snow-alb* simulation relative to the *baseline* simulation.

The *baseline* simulation had good to very good skill in simulating streamflow anomalies during pre-fire periods across the three study catchments (R^2=0.72-0.93; NSE = 0.70-0.93); however, *baseline* skill was largely degraded in post-fire years with consistent underestimates of post-fire streamflow anomalies. The fire-aware *Mod-params+GVF+Veg-class+Snow-alb* simulation significantly reduced post-fire streamflow anomaly underestimates by simulating enhanced streamflow. However, this fire-aware simulation maintains critical post-fire errors which were likely partially caused by inadequate fire perturbation treatments. The imposed fire perturbations had varying degrees of uncertainty from observationally-constrained (i.e., vegetation area reductions) to unconstrained guesses (i.e., assumed post-fire vegetation classification shifts) due to limited temporal and spatially representative information. Overall, the results from this research support that accounting for fire perturbations in LSMs can help reduce post-fire systematic biases, but applying fire-related perturbations to LSM simulations did not adequately resolve fire-induced model uncertainties. Therefore, accurately simulating terrestrial water and energy budgets in heavily burned catchments remains an open-ended challenge, and model-based analyses used to quantify fire-impacts on terrestrial water and energy budgets are likely limited to being interpreted as model responses, rather than true responses in nature until more sophisticated post-fire treatments for LSMs are developed.

Acknowledgements

This research was funded by California Department of Water Resources and the California State Water Project. We also acknowledge the support from NCAR Water System Program and NOAA MAPP Grant NA20OAR4310421. We also acknowledge the Airborne Snow Observatories, Inc. Grant 20220202-01 “Advancing Seasonal Water Supply Forecasting in the San Joaquin and Feather River Basins of California through Assimilation of Snowpack Information into the Community WRF-Hydro Model plus Optional State of Colorado ASO Assimilation and ESP Forecasting Research”. Cenlin He was partially supported by the NASA Early Career Investigator Program in Earth Science (ECIP-ES) Award 80NSSC24K1045. Special thanks and acknowledgements go to Kate Burchenal (Airborne Snow Observatory, Inc.) for aiding coordination and communication throughout the project.

REFERENCES

Abatzoglou, J.T., Battisti, D.S., Williams, A.P., Hansen, W.D., Harvey, B.J., Kolden, C.A., 2021. Projected increases in western US forest fire despite growing fuel constraints. *Commun Earth Environ* 2, 227. https://doi.org/10.1038/s43247-021-00299-0

Abolafia-Rosenzweig, R., Gochis, D., Schwarz, A., Painter, T., Deems, J., Dugger, A., Casali, M., & He, C. ,2024a. Sensitivity of WRF-Hydro terrestrial water budget simulations to fire disturbances in California's Feather River Basin. [Dataset]. Zenodo. https://doi.org/10.5281/zenodo.10655318

Abolafia-Rosenzweig, R., He, C., Chen, F., 2022a. Winter and spring climate explains a large portion of interannual variability and trend in western U.S. summer fire burned area. *Environ. Res. Lett*. 17, 054030. https://doi.org/10.1088/1748-9326/ac6886

Abolafia-Rosenzweig, R., He, C., Chen, F., Zhang, Y., Dugger, A., Livneh, B., Gochis, D., 2024b. Evaluating Noah-MP Simulated Runoff and Snowpack in Heavily Burned Pacific-Northwest Snow-Dominated Catchments. *JGR Atmospheres* 129, e2023JD039780. https://doi.org/10.1029/2023JD039780

Abolafia-Rosenzweig, R., He, C., McKenzie Skiles, S., Chen, F., Gochis, D., 2022b. Evaluation and Optimization of Snow Albedo Scheme in Noah-MP Land Surface Model Using In Situ Spectral Observations in the Colorado Rockies. *J Adv Model Earth Syst* 14. https://doi.org/10.1029/2022MS003141

Agbeshie, A.A., 2022. A review of the effects of forest fire on soil properties. *J. For. Res*. https://doi.org/10.1007/s11676-022-01475-4

Ahmad, S.K., et al., 2024. Droughts impede water balance recovery from fires in the Western United States. Nature Ecology & Evolution. https://doi.org/10.1038/s41559-023-02266-8

Atchley, A.L., Kinoshita, A.M., Lopez, S.R., Trader, L., Middleton, R., 2018. Simulating Surface and Subsurface Water Balance Changes Due to Burn Severity. *Vadose Zone Journal* 17, 1–13. https://doi.org/10.2136/vzj2018.05.0099

Bart, R. R., & Tague, C. L., 2017. The impact of wildfire on baseflow recession rates in California. *Hydrological Processes*, 31(8), 1662–1673. https://doi.org/10.1002/hyp.11141

Bond-Lamberty, B., Peckham, S.D., Gower, S.T., Ewers, B.E., 2009. Effects of fire on regional evapotranspiration in the central Canadian boreal forest. *Global Change Biology* 15, 1242–1254. https://doi.org/10.1111/j.1365-2486.2008.01776.x

Burles, K., Boon, S., 2011. Snowmelt energy balance in a burned forest plot, Crowsnest Pass, Alberta, Canada. *Hydrol. Process*. https://doi.org/10.1002/hyp.8067

Cardenas, M.B., 2014. Soil moisture variation and dynamics across a wildfire burn boundary in a loblolly pine (Pinus taeda) forest. *Journal of Hydrology*, 519, 490-502.

Chen, L., Berli, M., Chief, K., 2013. Examining modeling approaches for the rainfall-runoff process in wildfire-affected watersheds: using San Dimas Experimental Forest. *J. Am. Water Resour. Assoc*. 1–16. https://doi.org/10.1111/jawr.12043.

Cosgrove, B., et al., 2024. NOAA's National Water Model: Advancing operational hydrology through continental-scale modeling. *JAWRA Journal of the American Water Resources Association*.

Doerr, S.H., Shakesby, R.A., Walsh, R.P.D., 2000. Soil water repellency: its causes, characteristics and hydro-geomorphological significance. *Earth-Science Reviews*, 51(1-4), 33-65.

Ebel, B.A., 2019. Measurement Method Has a Larger Impact Than Spatial Scale For Plot-Scale Field-Saturated Hydraulic Conductivity (Kfs) After Wildfire and Prescribed Fire in Forests. *Earth Surface Processes and Landforms*, 44(10), 1945-1956.

Ebel, B.A., 2020. Temporal evolution of measured and simulated infiltration following wildfire in the Colorado Front Range, USA: Shifting thresholds of runoff generation and hydrologic hazards. *Journal of Hydrology* 585, 124765. https://doi.org/10.1016/j.jhydrol.2020.124765

Ebel, B.A., Martin, D.A., 2017. Meta-analysis of field-saturated hydraulic conductivity recovery following wildland fire: Applications for hydrologic model parameterization and resilience assessment. *Hydrological Processes* 31, 3682–3696. https://doi.org/10.1002/hyp.11288

Ebel, B.A., Moody, J.A., 2017. Synthesis of soil-hydraulic properties and infiltration timescales in wildfire-affected soils. Hydrological Processes, 31(2), 324-340.

Ebel, B.A., Moody, J.A., 2020. Parameter estimation for multiple post-wildfire hydrologic models. *Hydrological Processes*, 34(21), 4049-4066.

Eidenshink, J., Schwind, B., Brewer, K., Zhu, Z.-L., Quayle, B., Howard, S., 2007. A Project for Monitoring Trends in Burn Severity. fire ecol 3, 3–21. https://doi.org/10.4996/fireecology.0301003

Fall, G., et al., 2023. The Office of Water Prediction's Analysis of Record for Calibration, version 1.1: Dataset description and precipitation evaluation. *J American Water Resour Assoc* 1752–1688.13143. https://doi.org/10.1111/1752-1688.13143

Filipponi, F.; Valentini, E.; Nguyen Xuan, A.; Guerra, C.A.; Wolf, F.; Andrzejak, M.; Taramelli, A., 2018. Global MODIS Fraction of Green Vegetation Cover for Monitoring Abrupt and Gradual Vegetation Changes. *Remote Sens*. 10, 653. https://doi.org/10.3390/rs10040653

French N. H. F., Whitley M. A., Jenkins L. K., 2016. Fire disturbance effects on land surface albedo in Alaskan tundra. *J. Geophys. Res.Biogeosci*. 121, 841–854. doi: 10.1002/2015JG003177

Gersh, M., Gleason, K.E., Surunis, A., 2022. Forest Fire Effects on Landscape Snow Albedo Recovery and Decay. *Remote Sens*. *14*, 4079. https://doi.org/10.3390/rs14164079

Gleason, K.E., McConnell, J.R., Arienzo, M.M., Chellman, N., Calvin, W.M., 2019. Four-fold increase in solar forcing on snow in western U.S. burned forests since 1999. *Nat Commun* 10, 2026. https://doi.org/10.1038/s41467-019-09935-y

Gleason, K.E., Nolin, A.W., 2016. Charred forests accelerate snow albedo decay: parameterizing the post-fire radiative forcing on snow for three years following fire. *Hydrol. Process*. 30, 3855–3870. https://doi.org/10.1002/hyp.10897.

Gleason, K.E., Nolin, A.W., Roth, T.R., 2013. Charred forests increase snowmelt: Effects of burned woody debris and incoming solar radiation on snow ablation: charred forests increase snowmelt. *Geophys. Res. Lett*. 40, 4654–4661. https://doi.org/10.1002/grl.50896

Goeking, S.A., Tarboton, D.G., 2022. Variable Streamflow Response to Forest Disturbance in the Western US: A Large-Sample Hydrology Approach. *Water Resources Research* 58. https://doi.org/10.1029/2021WR031575

Goeking, S.A., Tarboton, D.G., 2020. Forests and Water Yield: A Synthesis of Disturbance Effects on Streamflow and Snowpack in Western Coniferous Forests. *Journal of Forestry* 118, 172–192. https://doi.org/10.1093/jofore/fvz069

Gochis, D.J., et al., 2020. The WRF-Hydro® modeling system technical description, (Version 5.2.0). NCAR Technical Note. 108 pages. Available online at: https://ral.ucar.edu/sites/default/files/public/projects/wrf-hydro/technical-description-user-guide/wrf-hydrov5.2technicaldescription.pdf.

Hampton, T.B., Basu, N.B., 2022. A novel Budyko-based approach to quantify post-forest-fire streamflow response and recovery timescales. *Journal of Hydrology* 608, 127685. https://doi.org/10.1016/j.jhydrol.2022.127685

Harpold, A.A., Biederman, J.A., Condon, K., Merino, M., Korgaonkar, Y., Nan, T., Sloat, L.L., Ross, M., Brooks, P.D., 2014. Changes in snow accumulation and ablation

following the Las Conchas Forest Fire, New Mexico, USA: changes in snow folloing fire. *Ecohydrol*. 7, 440–452. https://doi.org/10.1002/eco.1363

He, C., et al., 2023. The Community Noah-MP Land Surface Modeling System Technical Description Version 5.0, (No. NCAR/TN-575+STR), http://dx.doi.org/10.5065/ew8g-yr95

Kampf, S.K., McGrath, D., Sears, M.G., Fassnacht, S.R., Kiewiet, L., Hammond, J.C., 2022. Increasing wildfire impacts on snowpack in the western U.S. *Proc. Natl. Acad. Sci. USA* 119, e2200333119. https://doi.org/10.1073/pnas.2200333119

Kapnick, S.B., Yang, X., Vecchi, G.A., Delworth, T.L., Gudgel, R., Malyshev, S., Milly, P.C.D., Shevliakova, E., Underwood, S., Margulis, S.A., 2018. Potential for western US seasonal snowpack prediction. *Proc Natl Acad Sci USA* 115, 1180–1185. https://doi.org/10.1073/pnas.1716760115

Kinoshita, A.M., Hogue, T.S., Napper, C., 2014. Evaluating pre-and post-fire peak discharge predictions across western US watersheds. *JAWRA Journal of the American Water Resources Association* 50 (6), 1540–1557.

Koshkin, A.L., Hatchett, B.J., Nolin, A.W., 2022. Wildfire impacts on western United States snowpacks. *Front. Water* 4, 971271. https://doi.org/10.3389/frwa.2022.971271

Kumar, S.V., Holmes, T., Andela, N., Dharssi, I., Hain, C., Peters-Lidard, C., Mahanama, S.P., Arsenault, K.R., Nie, W., Getirana, A., 2021. The 2019–2020 Australian Drought and Bushfires Altered the Partitioning of Hydrological Fluxes. *Geophysical Research Letters*. e2020GL091411.

Larsen, I.J., MacDonald, L.H., Brown, E., Rough, D., Welsh, M.J., Pietraszek, J.H., Libohova, Z., 2009. Causes of Post-Fire Runoff and Erosion: Water Repellency, Cover, or Soil Sealing? *Soil Science Society of America Journal*, 73(4), 1393-1407.

Li, C., Handwerger, A.L., Wang, J., Yu, W., Li, X., Finnegan, N.J., Xie, Y., Buscarnera, G., Horton, D.E., 2022. Augmentation of WRF-Hydro to simulate overland-flow- and streamflow-generated debris flow susceptibility in burn scars. *Nat. Hazards Earth Syst. Sci*, *22*(7), 2317-2345.

Li, D., Wrzesien, M.L., Durand, M., Adam, J., Lettenmaier, D.P., 2017. How much runoff originates as snow in the western United States, and how will that change in the future? *Geophys. Res. Lett*. 44, 6163–6172. https://doi.org/10.1002/2017GL073551

Li, L., Yang, Z., Matheny, A.M., Zheng, H., Swenson, S.C., Lawrence, D.M., Barlage, M., Yan, B., McDowell, N.G., Leung, L.R., 2021. Representation of Plant Hydraulics in

the Noah-MP Land Surface Model: Model Development and Multiscale Evaluation. *J. Adv. Model. Earth Syst.* 13. https://doi.org/10.1029/2020MS002214

López-Vicente, M., 2020. Forest fire effects on sediment connectivity in headwater sub-catchments: Evaluation of indices performance. *Science of the Total Environment*, 732, 139206.

Lu, B., Zhong, J., Wang, W., Tang, S., Zheng, Z., 2021. Influence of Near Real-Time Green Vegetation Fraction Data on Numerical Weather Prediction by WRF over North China. *Journal of Meteorological Research* 35.

Maina, F.Z., Siirila-Woodburn, E.R., 2020. Watersheds dynamics following wildfires: Nonlinear feedbacks and implications on hydrologic responses. *Hydrological Processes* 34, 33–50. https://doi.org/10.1002/hyp.13568

Martin, D.A., Moody, J.A., 2001. Comparison of soil infiltration rates in burned and unburned mountainous watersheds. *Hydrol. Process*. 15, 2893–2903. https://doi.org/10.1002/hyp.380

Maxwell, J., St Clair, S.B., 2019. Snowpack properties vary in response to burn severity gradients in montane forests. *Environ. Res. Lett*. 14, 124094. https://doi.org/10.1088/1748-9326/ab5de8

Moody, J.A., 2013. Current research issues related to post-wildfire runoff and erosion processes. *Earth-Science Reviews*, 122, 10-37.

Moody, J.A., Ebel, B.A., Nyman, P., Martin, D.A., Stoof, C.R., McKinley, R., 2015. Relations between soil hydraulic properties and burn severity. *International Journal of Wildland Fire* 25.3. 279-293.

Moody, J.A., Kinner, D.A., 2005. Spatial structures of stream and hillslope drainage networks following gully erosion after wildfire. Earth Surface Processes and Landforms: *The Journal of the British Geomorphological Research Group*, 31(3), 319-337.

Moody, J.A., Martin, D.A., Haire, S.L., Kinner, D.A., 2008. Linking runoff response to burn severity after a wildfire. *Hydrol. Process*. 22, 2063–2074. https://doi.org/10.1002/hyp.6806

Moriasi, D.N., Arnold, J.G., Liew, M.W.V., Bingner, R.L., Harmel, R.D., Veith, T.L., 2007. Model evaluation guidelines for systematic quantification of accuracy in watershed simulations. *Transactions of the ASABE* 50.3. 885-900.

Moriasi, D.N., Gitau, M.W., Pai, N., Daggupati, P., 2015. Hydrologic and water quality models: Performance measures and evaluation criteria. *Transactions of the ASABE* 58.6 (2015): 1763-1785.

Mu, M., Kauwe, M.G.D., Ukkola, A.M., Pitman, A.J., Gimeno, T.E., Medlyn, B.E., Or, D., Yang, J., Ellsworth, D.S., 2021. Evaluating a land surface model at a water-limited site: implications for land surface contributions to droughts and heatwaves. *Hydrol. Earth Syst. Sci*, *2020*, 1-38.

Myneni, R., Knyazikhin, Y., Park, T. (2015). MOD15A2H MODIS Leaf Area Index/FPAR 8-Day L4 Global 500m SIN Grid V006. NASA EOSDIS Land Processes DAAC. http://doi.org/10.5067/MODIS/MOD15A2H.006 (Terra) http://doi.org/10.5067/MODIS/MYD15A2H.006 (Aqua)

Myneni, R.B., Williams, D.L., 1994. On the relationship between FAPAR and NDVI. Remote Sens. Environ. 49, 200–211. https://doi.org/10.1016/0034-4257(94) 90016-7.

Niemeyer, R.J., Bladon, K.D., Woodsmith, R.D., 2020. Long-term hydrologic recovery after wildfire and post-fire forest management in the interior Pacific Northwest. *Hydrological Processes* 34, 1182–1197. https://doi.org/10.1002/hyp.13665

Niu, G.-Y., Yang, Z.-L., Mitchell, K.E., Chen, F., Ek, M.B., Barlage, M., Kumar, A., Manning, K., Niyogi, D., Rosero, E., Tewari, M., Xia, Y., 2011. The community Noah land surface model with multiparameterization options (Noah-MP): 1. Model description and evaluation with local-scale measurements. *J. Geophys. Res*. 116, D12109. https://doi.org/10.1029/2010JD015139

Painter, T.H., et al., 2016. The Airborne Snow Observatory: Fusion of scanning lidar, imaging spectrometer, and physically-based modeling for mapping snow water equivalent and snow albedo. *Remote Sensing of Environment*, 184, 139-152.

Partington, D., Thyer, M., Shanafield, M., McInerney, D., Westra, S., Maier, H., Simmons, C., Croke, B., Jakeman, A.J., Gupta, H., Kavetski, D., 2022. Predicting wildfire induced changes to runoff: A review and synthesis of modeling approaches. *WIREs Water* 9. https://doi.org/10.1002/wat2.1599

Pugh, E., Gordon, E., 2013. A conceptual model of water yield effects from beetle-induced tree death in snow-dominated lodgepole pine forests: A Conceptual Model of the Water Yield Effects of Tree Death. *Hydrol. Process*. 27, 2048–2060. https://doi.org/10.1002/hyp.9312

Safford, H.D., Miller, J., Schmidt, D., Roath, B., Parsons, A., 2008. BAER Soil Burn Severity Maps Do Not Measure Fire Effects to Vegetation: A Comment on Odion and Hanson (2006). *Ecosystems* 11, 1–11. https://doi.org/10.1007/s10021-007-9094-z

Schaake, J.C., Koren, V.I., Duan, Q.-Y., Mitchell, K., Chen, F., 1996. Simple water balance model for estimating runoff at different spatial and temporal scales. *Journal of Geophysical Research: Atmospheres*, 101(D3), 7461-7475.

Seibert, J., McDonnell, J.J., Woodsmith, R.D., 2010. Effects of wildfire on catchment runoff response: a modelling approach to detect changes in snow-dominated forested catchments. *Hydrology Research* 41, 378–390. https://doi.org/10.2166/nh.2010.036

Shakesby, R., Doerr, S., 2006. Wildfire as a hydrological and geomorphological agent. *Earth-Science Reviews* 74, 269–307. https://doi.org/10.1016/j.earscirev.2005.10.006

Smoot, E.E. and Gleason, K.E., 2021. Forest Fires Reduce Snow-Water Storage and Advance the Timing of Snowmelt across the Western U.S. *Water*, 13, 3533. https://doi.org/10.3390/w13243533

Spence, C., Hedstrom, N., Tank, S.E., Quinton, W.L., Olefeldt, D., Goodman, S., Dion, N., 2020. Hydrological resilience to forest fire in the subarctic Canadian shield. *Hydrological Processes* 34, 4940–4958. https://doi.org/10.1002/hyp.13915

Stoof, C.R., Ferreira, A.J.D., Mol, W., Drooger, S., Slingerland, E.C., Mansholt, A.U., Ferreira, C.S.S., Ritsema, C.J., 2015. Soil surface changes increase runoff and erosion risk after a low–moderate severity fire. *Geoderma*, 239, 58-67.

Stoof, C.R., Vervoort, R.W., Iwema, J., van den Elsen, E., Ferreira, A.J.D., Ritsema, C.J., 2012. Hydrological response of a small catchment burned by experimental fire. *Hydrol. Earth Syst. Sci*. 16, 267–285. https://doi.org/10.5194/hess-16-267-2012

Ukkola, A.M., Pitman, A.J., Decker, M., Kauwe, M.G.D., Abramowitz, G., Kala, J., Wang, Y.-P., 2016. Modelling evapotranspiration during precipitation deficits: identifying critical processes in a land surface model. *Hydrol. Earth Syst. Sci*, 20(6), 2403-2419.

Veraverbeke, S., Verstraeten, W.W., Lhermitte, S., 2012. Assessment of post-fire changes in land surface temperature and surface albedo, and their relation with fire–burn severity using multitemporal MODIS imagery. *International Journal of Wildland Fire* 21.3. 243-256.

Verma, S., Jayakumar, S., 2012. Impact of forest fire on physical, chemical and biological properties of soil: A review. *proceedings of the International Academy of Ecology and Environmental Sciences*, 2(3), 168.

Viviroli, D., Dürr, H.H., Messerli, B., Meybeck, M., Weingartner, R., 2007. Mountains of the world, water towers for humanity: Typology, mapping, and global significance: Mountains as Water Towers for Humanity. *Water Resour. Res*. 43. https://doi.org/10.1029/2006WR005653

Wang, Y., 2020. Quantifying the effects of environmental factors on wildfire burned area in the south central US using integrated machine learning techniques. *Atmos. Chem. Phys*, 20(18), 11065-11087.

Williams, A.P., Livneh, B., McKinnon, K.A., Hansen, W.D., Mankin, J.S., Cook, B.I., Smerdon, J.E., Varuolo-Clarke, A.M., Bjarke, N.R., Juang, C.S., Lettenmaier, D.P., 2022. Growing impact of wildfire on western US water supply. *Proc Natl Acad Sci USA* 119, e2114069119. https://doi.org/10.1073/pnas.2114069119

Xiao, M., Mahanama, S.P., Xue, Y., Chen, F., Lettenmaier, D.P., 2021. Modeling Snow Ablation over the Mountains of the Western United States: Patterns and Controlling Factors. *Journal of Hydrometeorology* 22, 297–311. https://doi.org/10.1175/JHM-D-19-0198.1

Yang, Z.-L., Dickinson, R. E., Robock, A., & Vinnikov, K. Y., 1997. Validation of the snow submodel of the biosphere-atmosphere transfer scheme with Russian snow cover and meteorological observational data. *Journal of Climate*, 10(2), 353–373. https://doi.org/10.1175/1520-0442(1997)010<0353:VOTSSO>2.0.CO;2

Figure captions

Figure 1. Study domain. **(a)** Perimeters of catchments (black lines), study gauge locations (NFP, MER, ICR; black dots), fire areas (red shading), the Feather River (bold blue line), and Lake Oroville (blue shading in southwest corner of the domain). Fire burn severity maps are shown for the **(b)** Walker Fire ignited in Sept. 2019 and contained in Jan. 2020, **(c)** Sugar Fire ignited in Jul. 2021 and contained in Nov. 2021, **(d)** North Complex Fire ignited in Aug. 2020 and contained in Dec. 2020, **(e)** Camp Fire ignited and contained in November 2018 and **(f)** Dixie Fire ignited in Jul. 2021 and contained in Oct. 2021.

Figure 2. (a) Annual time series of maximum Fraction of Photosynthetically Active Radiation (FPAR) observed by MODIS spatially averaged across fire perimeters of the North Complex, Camp, Walker, Sugar and Dixie fire events, respectively. **(b)** MODIS-based fractional green vegetation fraction (GVF) changes applied in the WRF-Hydro experiments accounting for fire impacts on GVF (eq. 1; Table 1).

Figure 3. Observed visible snow albedo from an ASO survey over the Feather River Basin for March 31 – April 2, 2022 **(a)** outside of fire scars and **(b)** inside of fire scars. Corresponding snow albedo biases from the WRF-Hydro *baseline* simulation **(c)** outside of fire scars and **(d)** inside of fire scars.

Figure 4. Comparisons between simulated and observed daily streamflow (Q) anomalies during **(a,c,e)** pre-fire and **(b,d,f)** post-fire years at the MER, NFP and ICR stations. Metrics related to the *baseline* and *Mod-params+GVF+Veg-class+Snow-alb* simulation are reported in blue and red, respectively. Pre- and post-fire periods for MFF, NFF and EBNFF are described in Section 2.3.

Figure 5. (a-c) Muliyear mean (2000-2022) daily streamflow (Q) at stations denoted in column titles (see Figure 1 for station locations) from the 5 WRF-Hydro experiments (Table 1) at the three study catchments. **(d-f)** corresponding difference plots relative to the *baseline* experiment which does not apply fire perturbations.

Figure 6. (a-c) Muliyear mean (2000-2022) daily subsurface flow spatially averaged across study catchments from the 5 WRF-Hydro experiments (Table 1). **(d-f)** corresponding difference plots relative to the *baseline* experiment which does not apply fire perturbations.

Figure 7. (a-c) Muliyear mean (2000-2022) daily evapotranspiration (ET) spatially averaged across study catchments from the 5 WRF-Hydro experiments (Table 1). **(d-f)** corresponding difference plots relative to the *baseline* experiment which does not apply fire perturbations.

Figure 8. Multiyear mean daily evapotranspiration (ET) from the *baseline* simulation averaged during **(a)** fall (SON), **(b)** winter (DJF), **(c)** spring (MAM) and **(d)** summer (JJA). **(e-h)** corresponding differences between *Mod-params+GVF+Veg-class+Snow-alb* and *baseline* simulated ET.

Figure 9. Comparison of evapotranspiration (ET) partitions —transpiration (E_{tran}), canopy evaporation (E_{can}) and bare ground evaporation plus sublimation (E_{dir})—from the *Mod-params+ GVF+Veg-class+Snow-alb* and *baseline* simulations. Top row **(a-c)** shows multiyear (2000-2022) daily means for each component at the three study catchments. **(d-f)** shows the differences between the three ET partitions as *Mod-params+GVF+Veg-class+Snow-alb* minus *baseline*.

Figure 10. (a-c) Muliyear mean (2000-2022) daily snow water equivalent (SWE) spatially averaged across study catchments from the 5 WRF-Hydro experiments (Table 1). **(d-f)** corresponding difference plots relative to the *baseline* experiment which does not apply fire perturbations.

Figure 11. Multiyear mean daily snow water equivalent (SWE) from the *baseline* simulation averaged during **(a)** fall (SON), **(b)** winter (DJF), **(c)** spring (MAM) and **(d)** summer (JJA). **(e-h)** corresponding differences between *Mod-params + GVF + Veg-class + Snow-alb* and *baseline* simulated SWE.

Figure 12. (a-c) Muliyear mean (2000-2022) daily soil moisture (SM) spatially averaged across study catchments from the 5 WRF-Hydro experiments (Table 1). **(d-f)** corresponding difference plots relative to the *baseline* experiment which does not apply fire perturbations.
Figure 13. Multiyear mean daily soil moisture (SM) from the *baseline* simulation averaged during **(a)** fall (SON), **(b)** winter (DJF), **(c)** spring (MAM) and **(d)** summer (JJA). **(e-h)**

corresponding differences between *Mod-params+GVF+Veg-class+Snow-alb* and *baseline* simulated SWE.

Novelty Statement

To the authors' knowledge this is the first research publication to include the following elements:

(i) Explicitly account for a suite of fire perturbations to the land surface in the operationally used WRF-Hydro modeling system and the Noah-MP land surface model.
(ii) Incrementally apply fire perturbations to quantify simulated fire impacts on land surface hydrology from each perturbation and perturbations in combination.
(iii) Account for fire-enhanced snow albedo degradation in a physically based modeling system considering observed fire impacts on snow albedo from measurements from the Airborne Snow Observatory (ASO).
(iv) Quantify simulated fire impacts on water supply in a snow-dominated river basin that is the primary source for a State Water Project.
(v) Validation of physically based simulations from the WRF-Hydro modeling system in pre- and post-fire periods using configurations that include and neglect fire impacts.

These novel contributions are used to (i) quantify the sensitivity of fire perturbations in the operationally used WRF-Hydro modelling system over the heavily burned and snow-dominated Feather River Basin which is the primary source for California's State Water Project, and (ii) evaluate if explicitly accounting for fire perturbations in WRF-Hydro enhances post-fire streamflow modelling accuracy. This study highlights the importance of accounting for fire perturbations in physically based hydrologic modeling systems while providing a novel methodology designed to account for fire impacts that improves simulated streamflow accuracy in burned catchments during post-fire periods.

WRF-Hydro simulates fire-enhanced streamflow, reducing post-fire model anomaly biases. **(a)** perimeters of study catchments in the Feather River Basin, study gauge locations (black dots) and fire areas (red shading). **(b,c,d)** Muliyear mean (2000-2022) daily streamflow (Q) from a no-fire baseline simulation (black lines) and a fire-aware simulation (red lines) that accounts for fire impacts on soil and routing parameters, vegetation area and classifications and snow albedo; anomaly biases in black and red text are for baseline and fire-aware simulations, respectively.

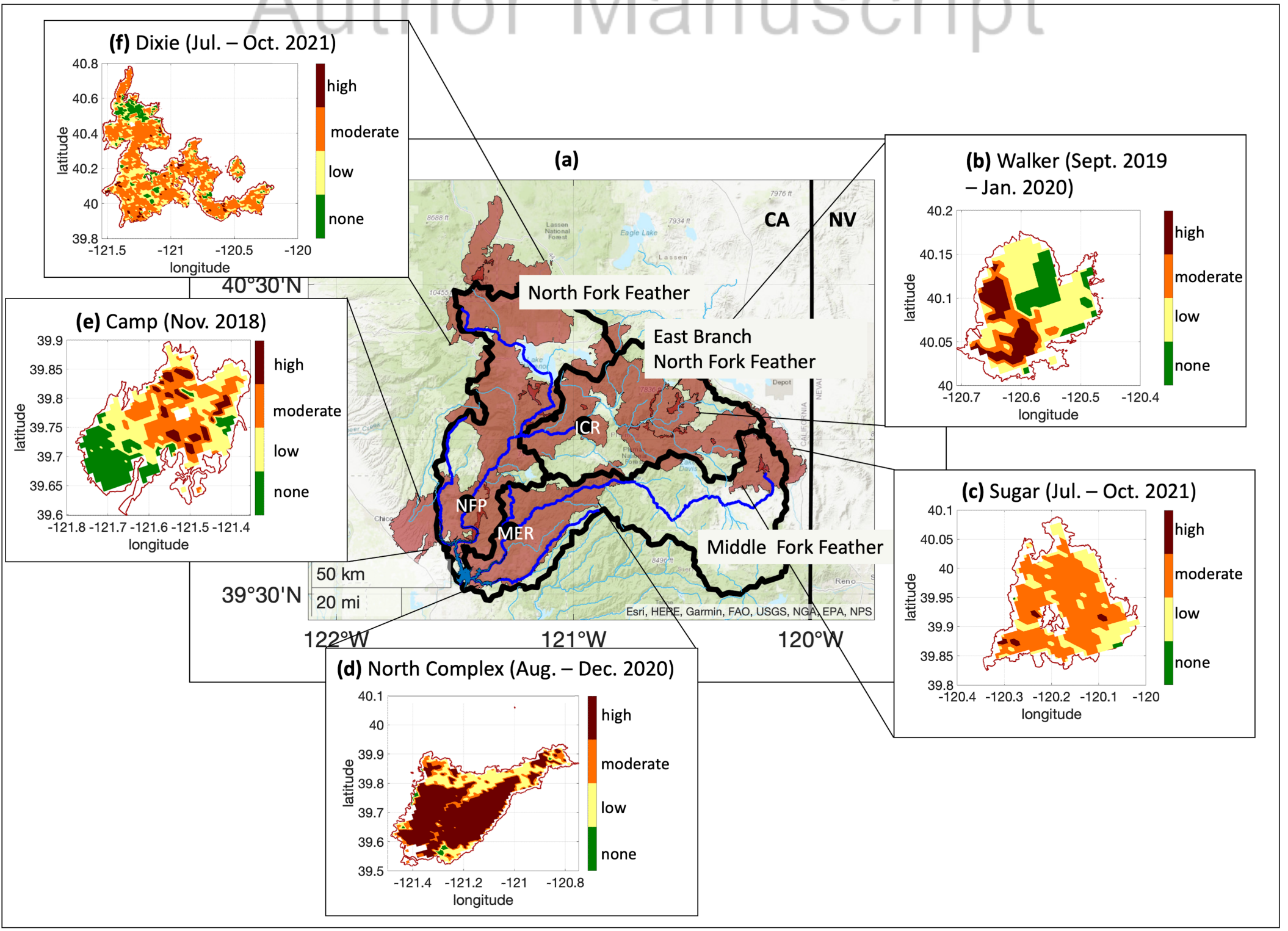

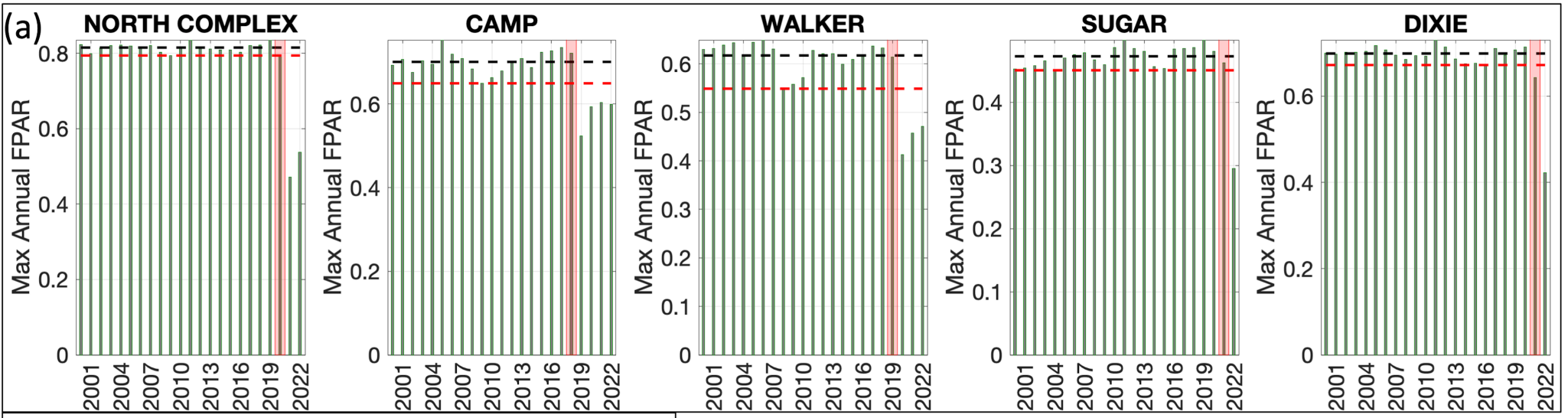

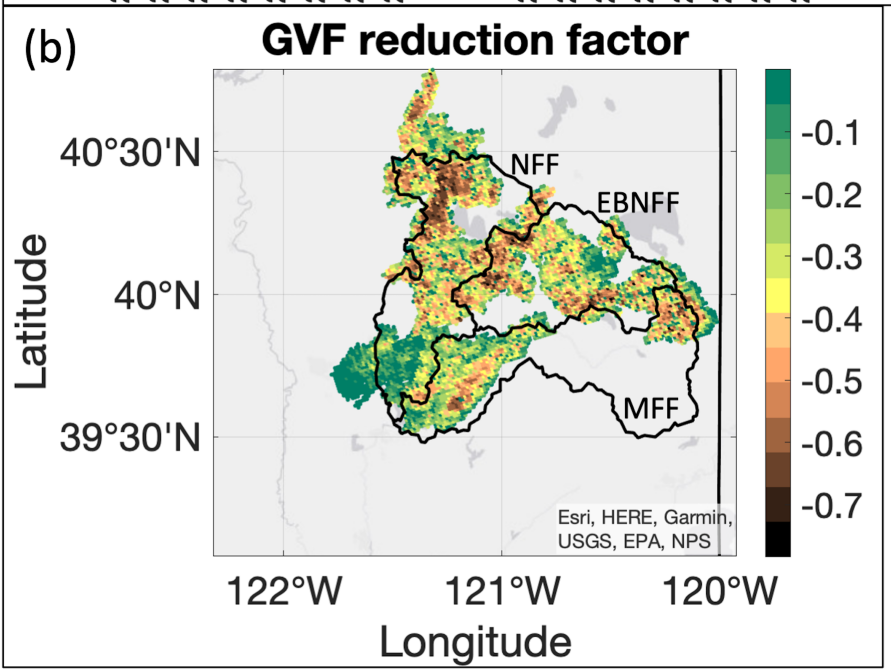

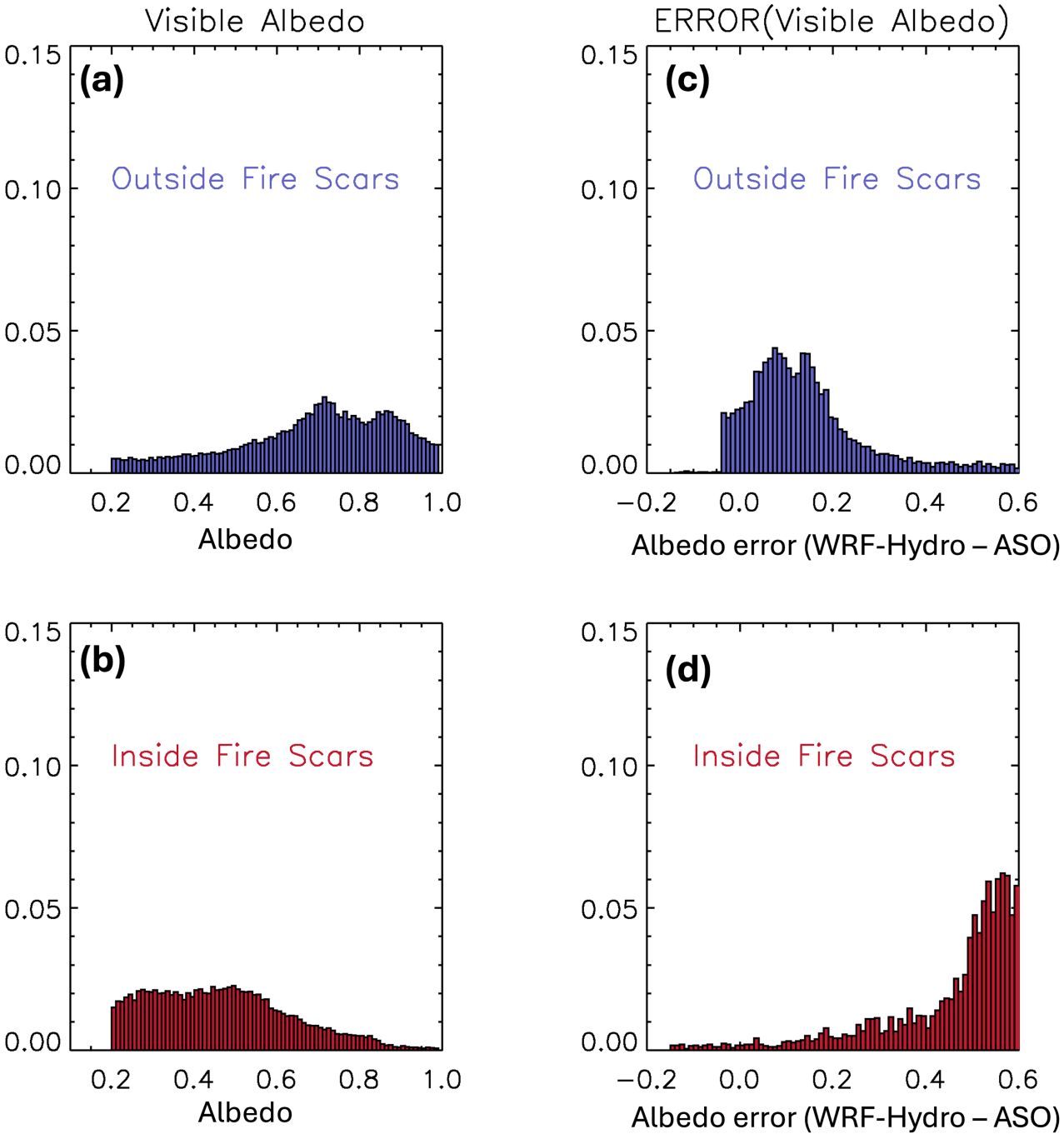

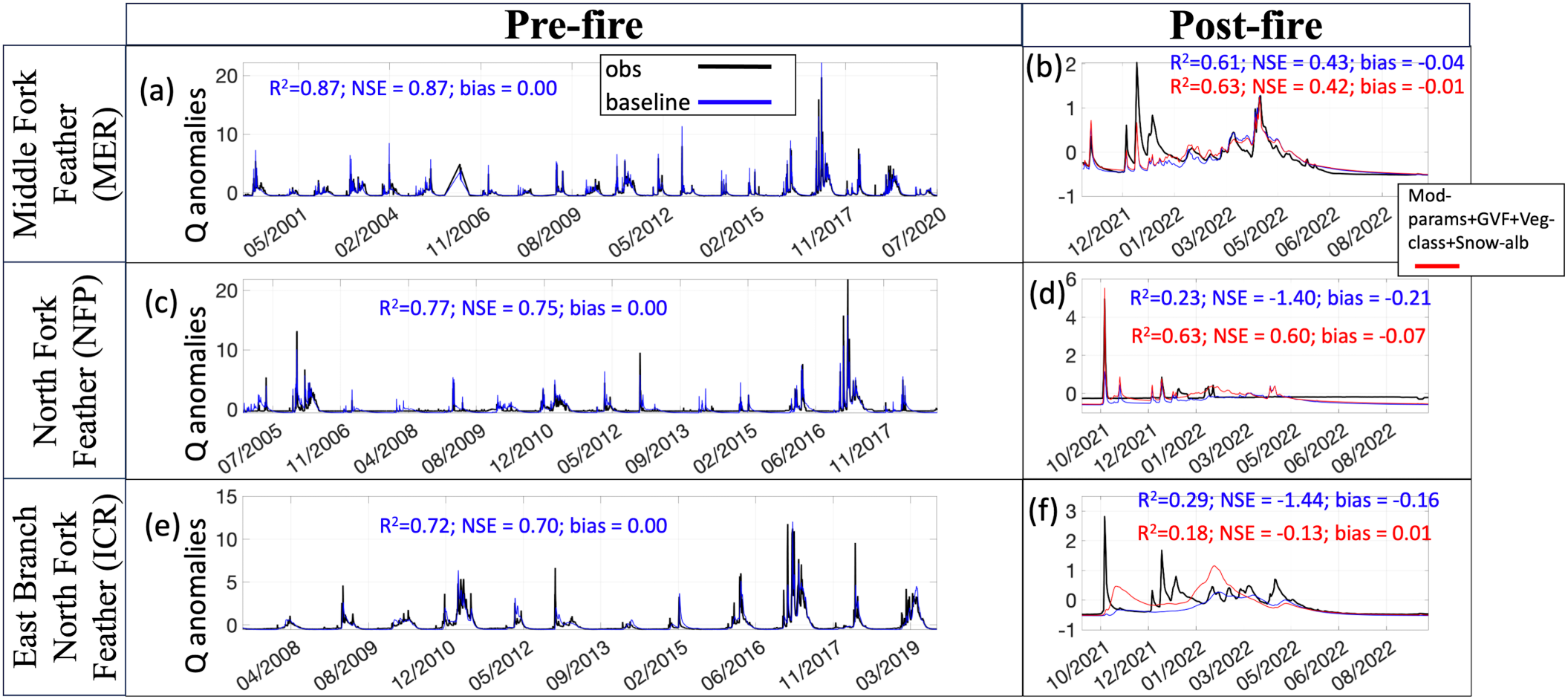

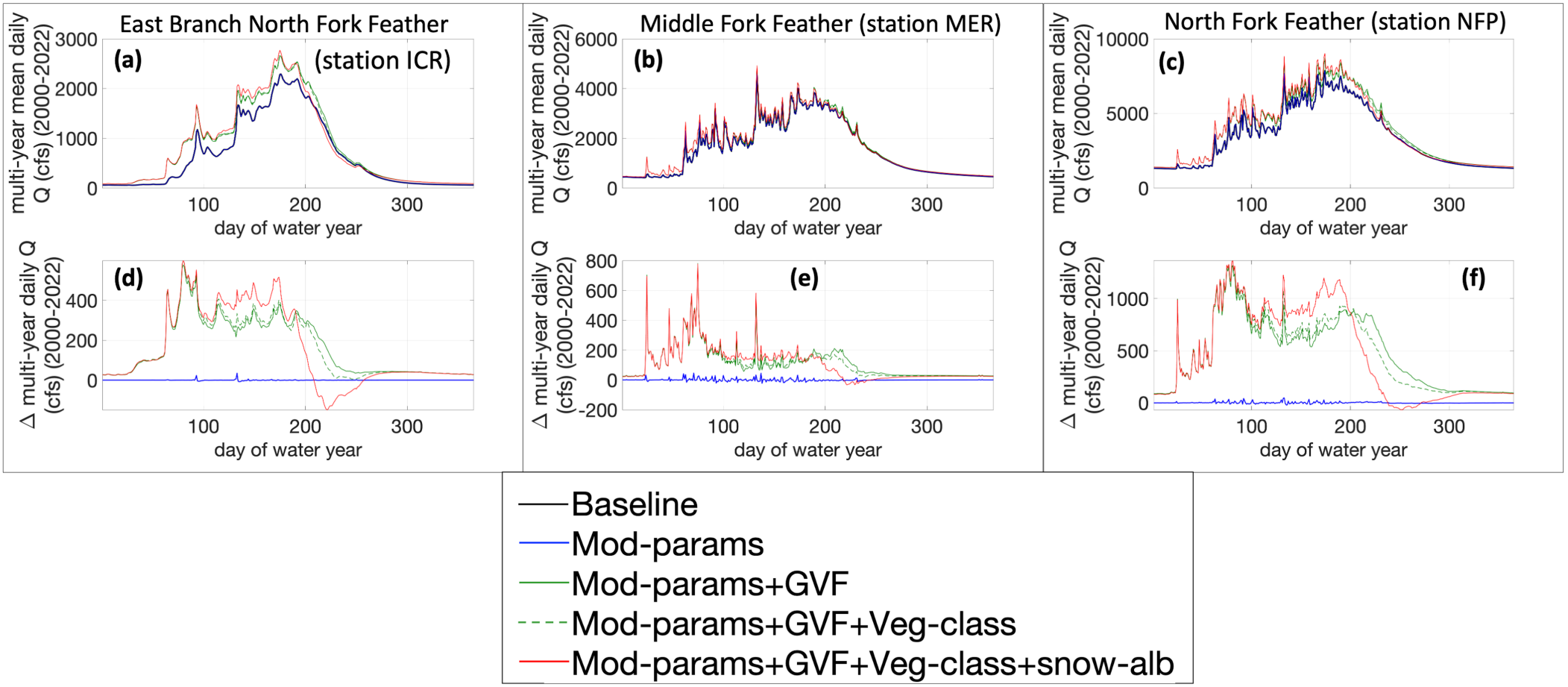

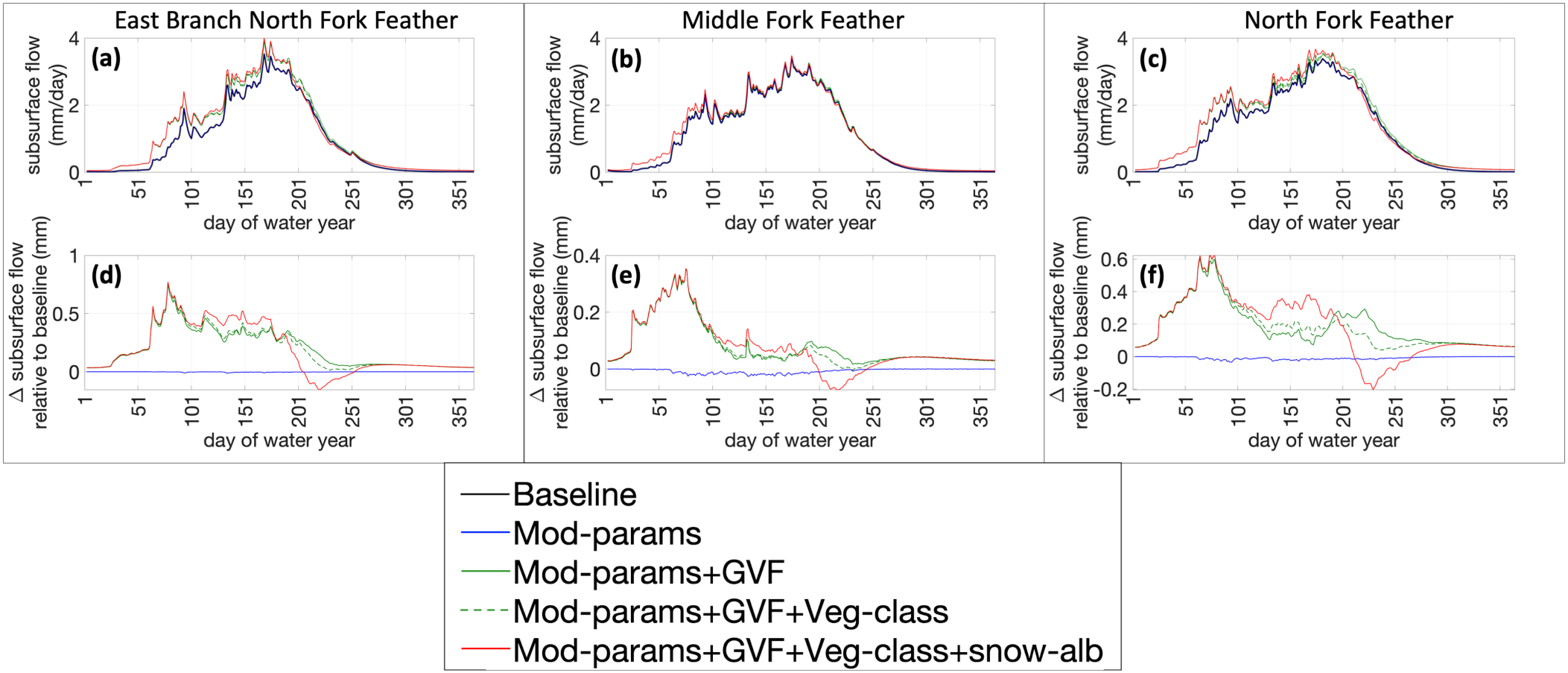

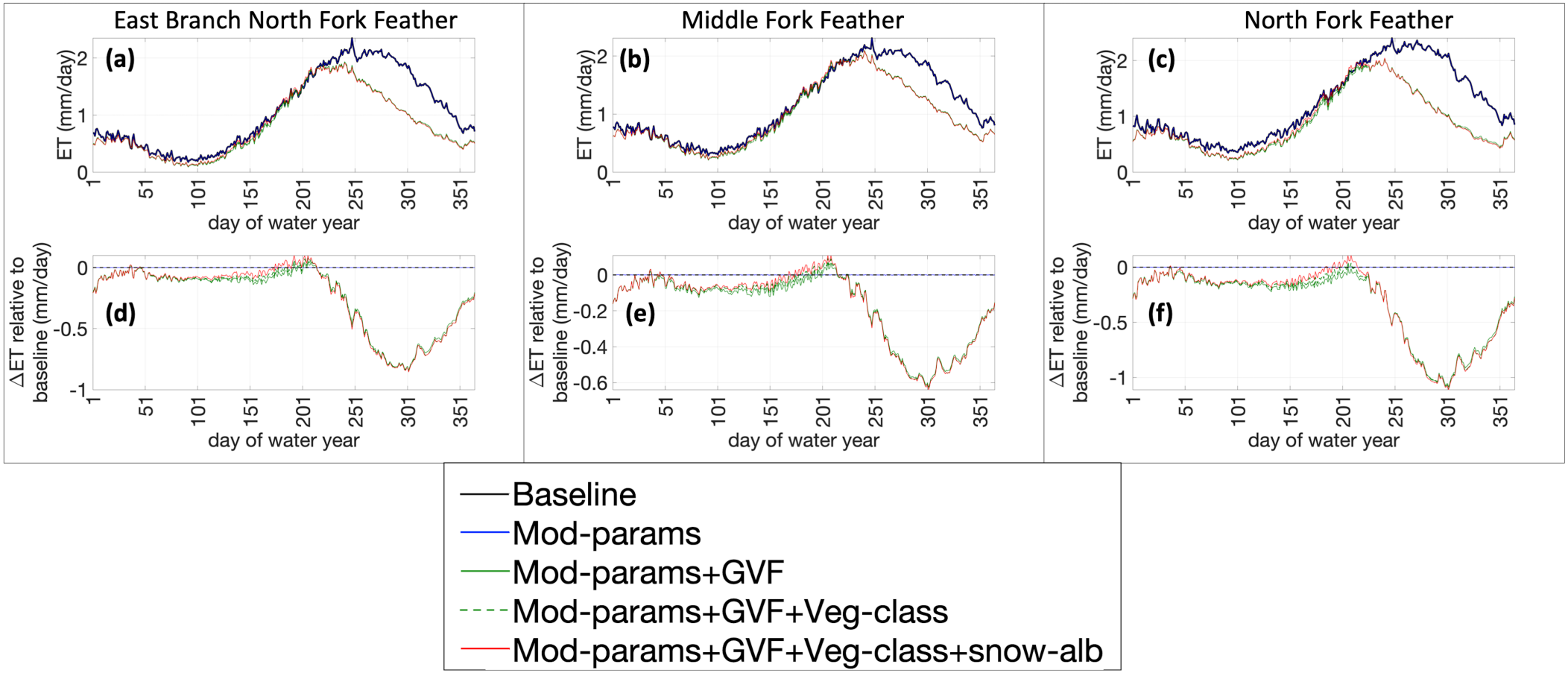

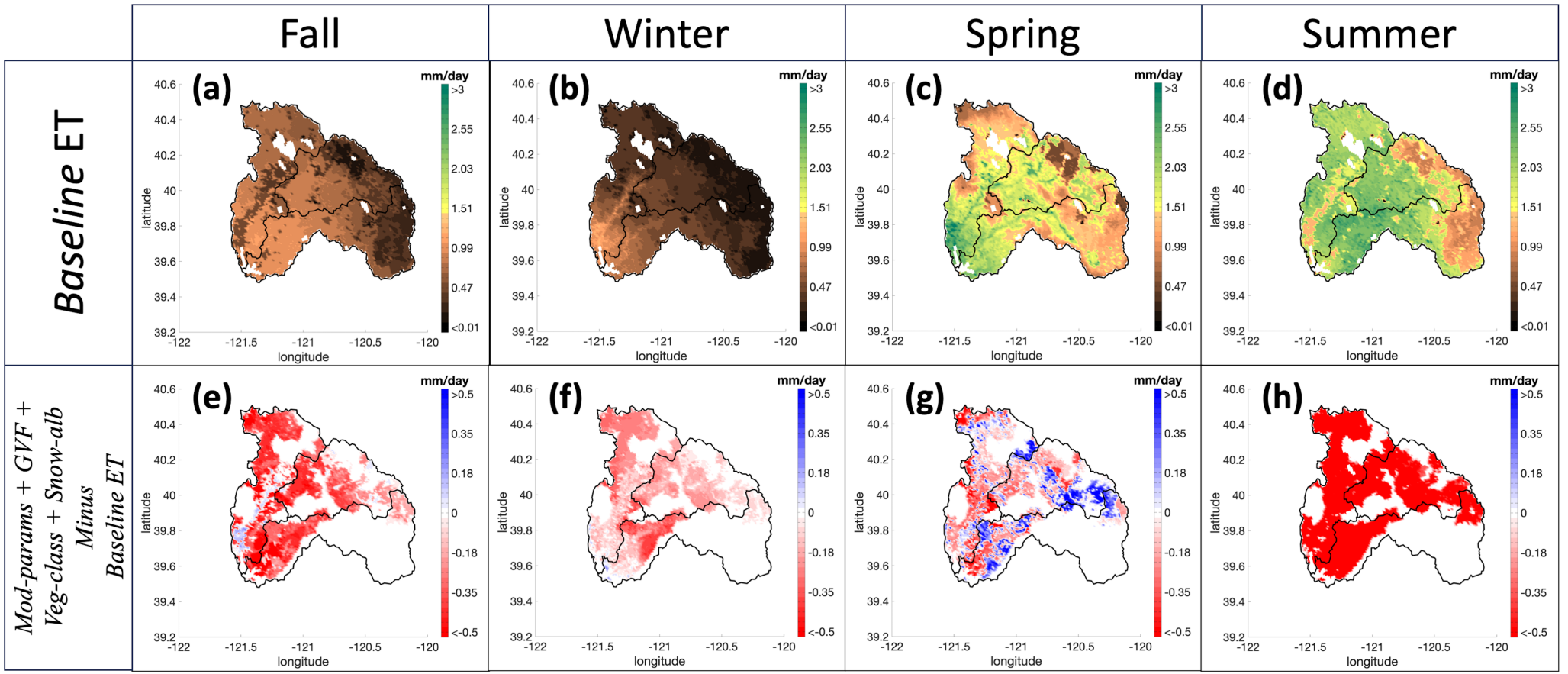

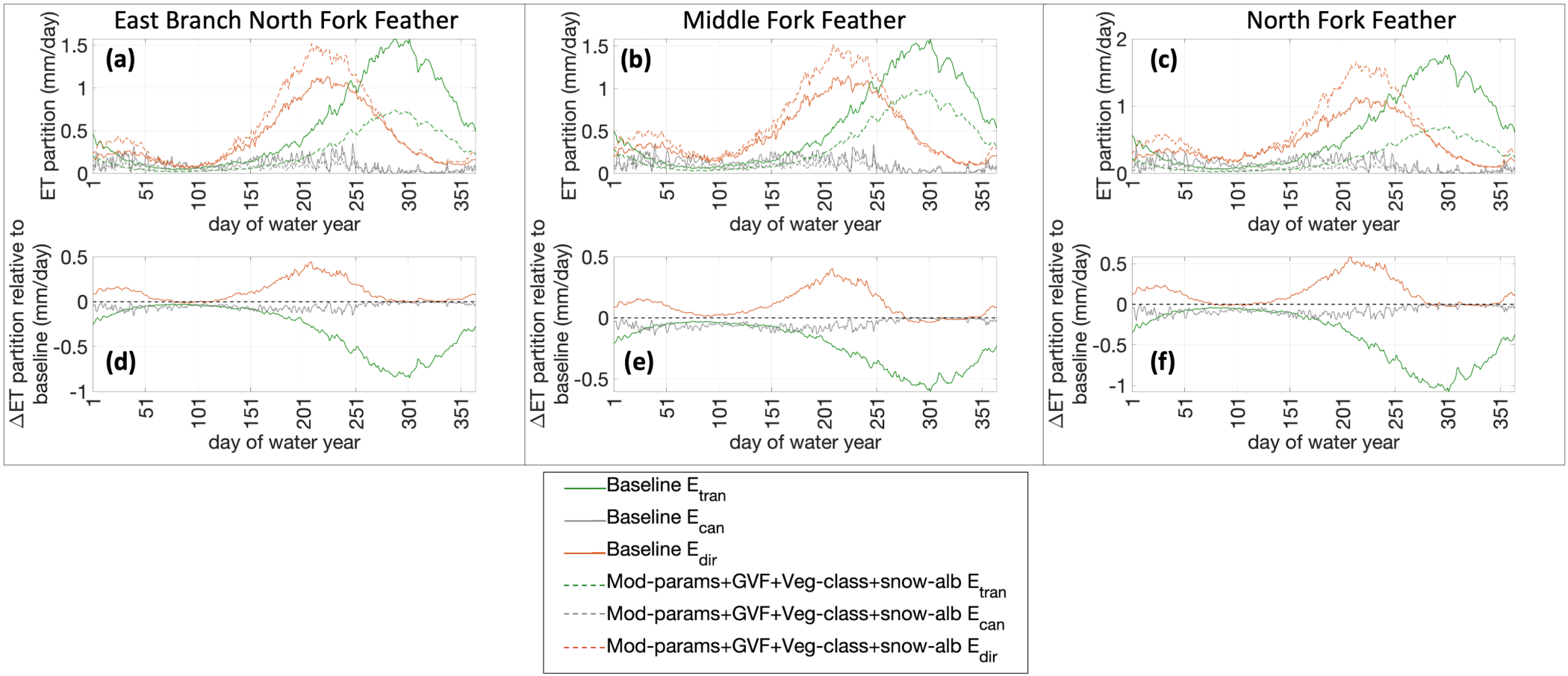

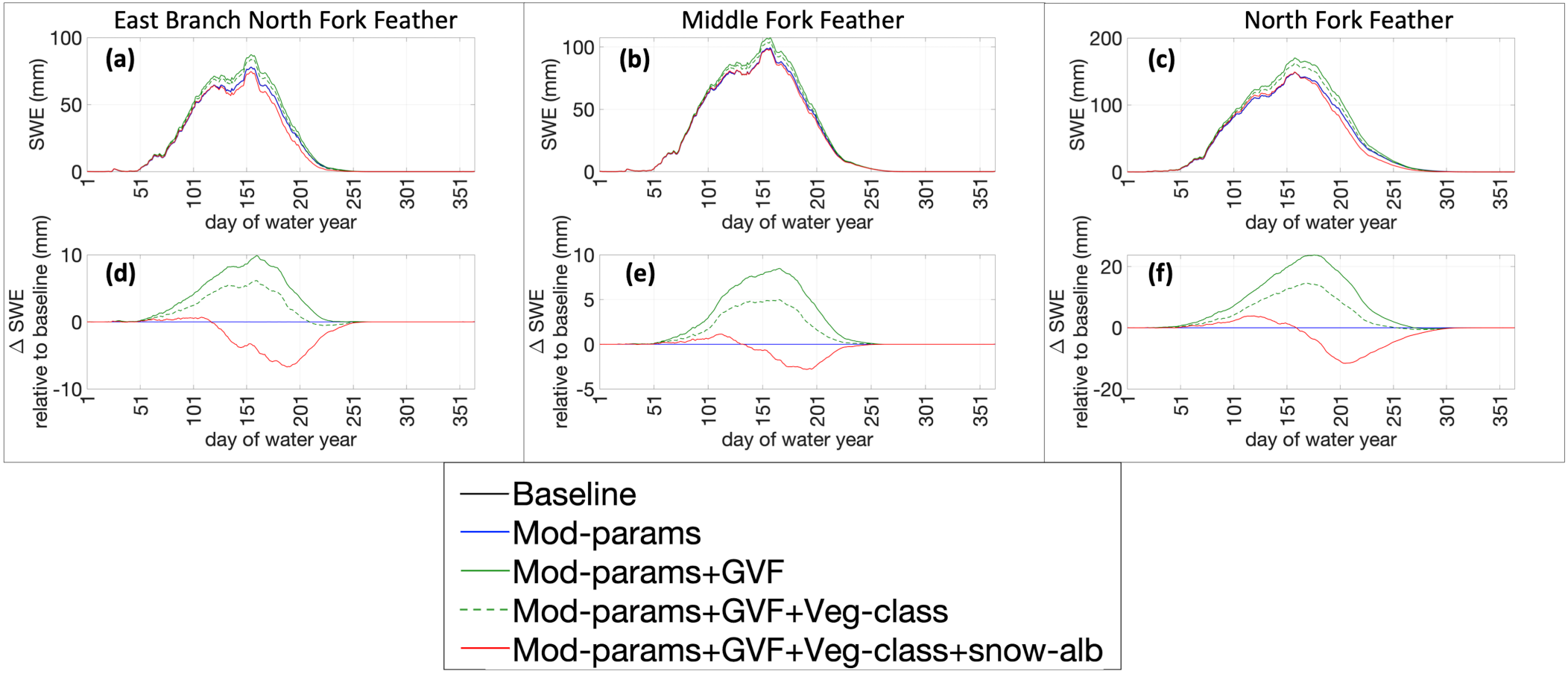

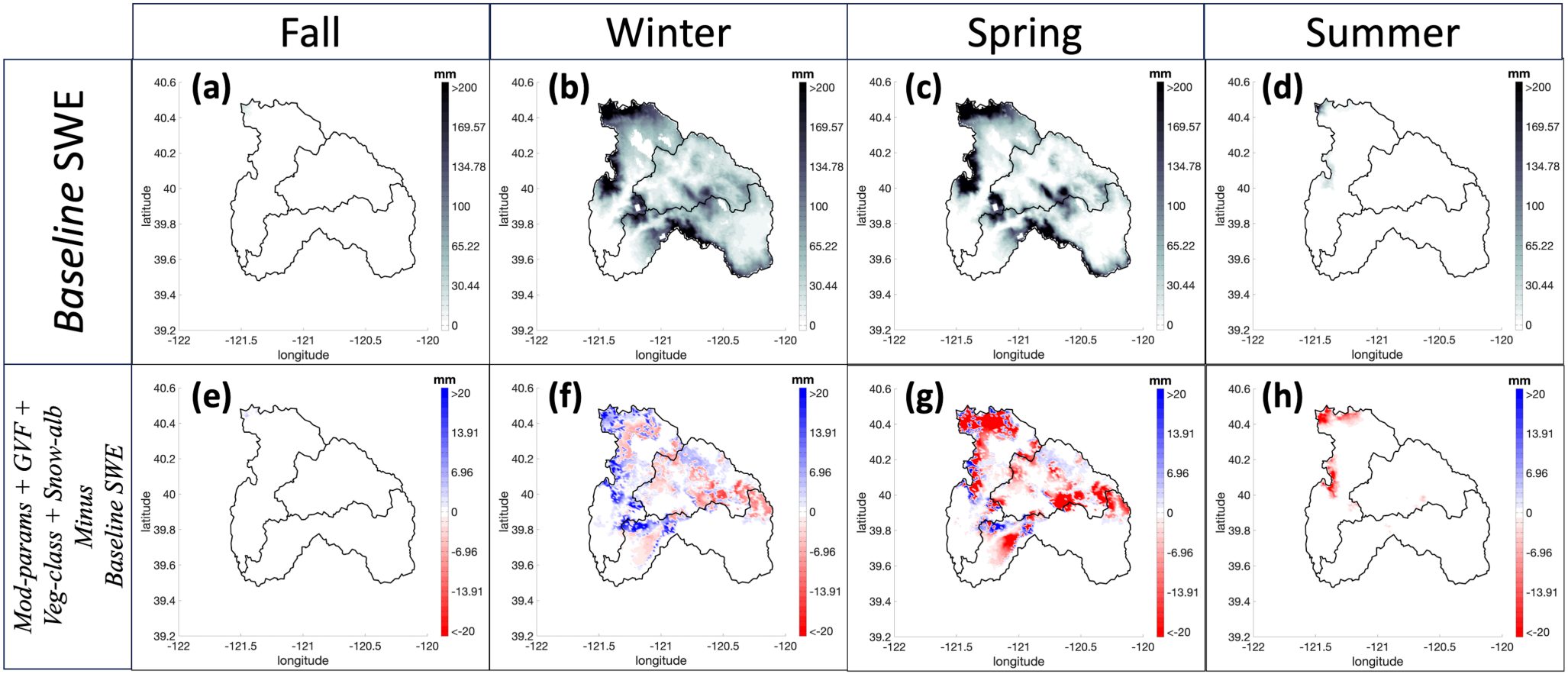

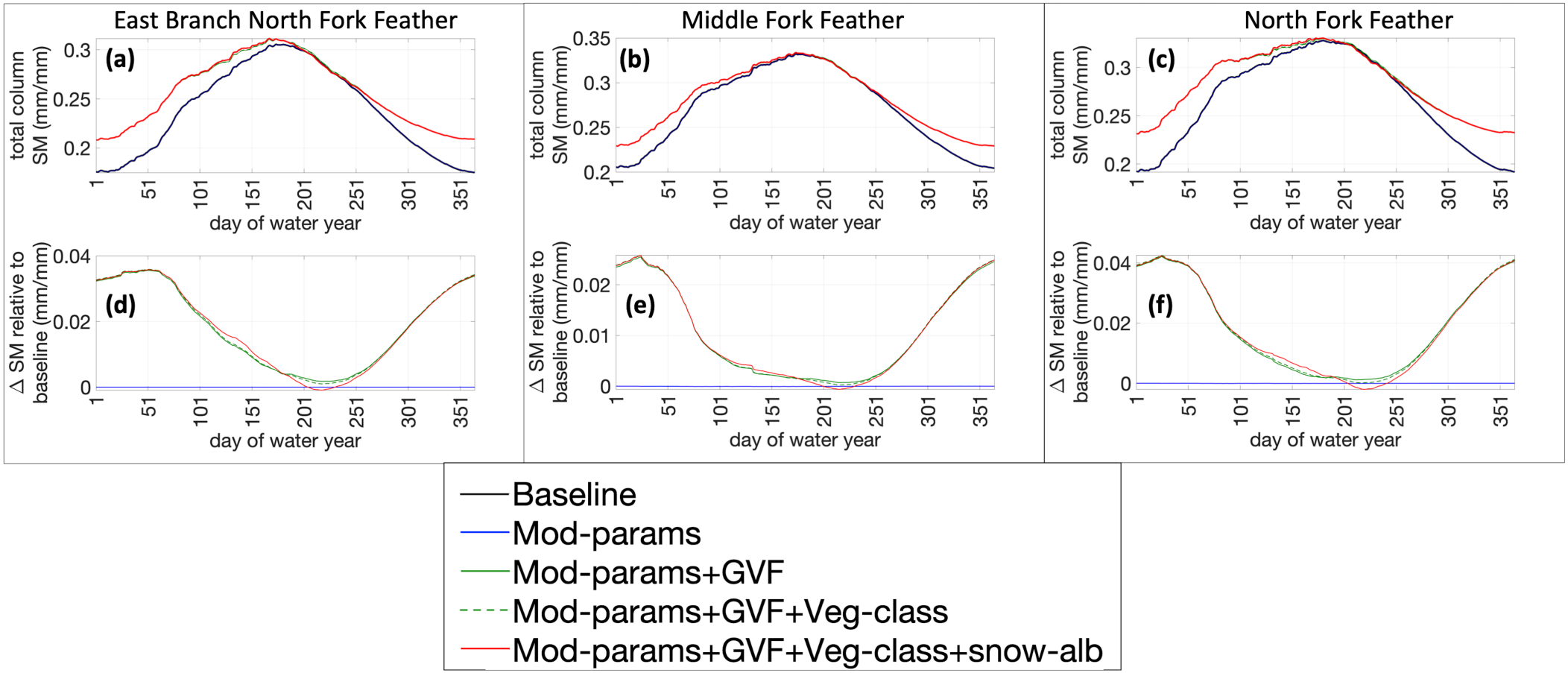

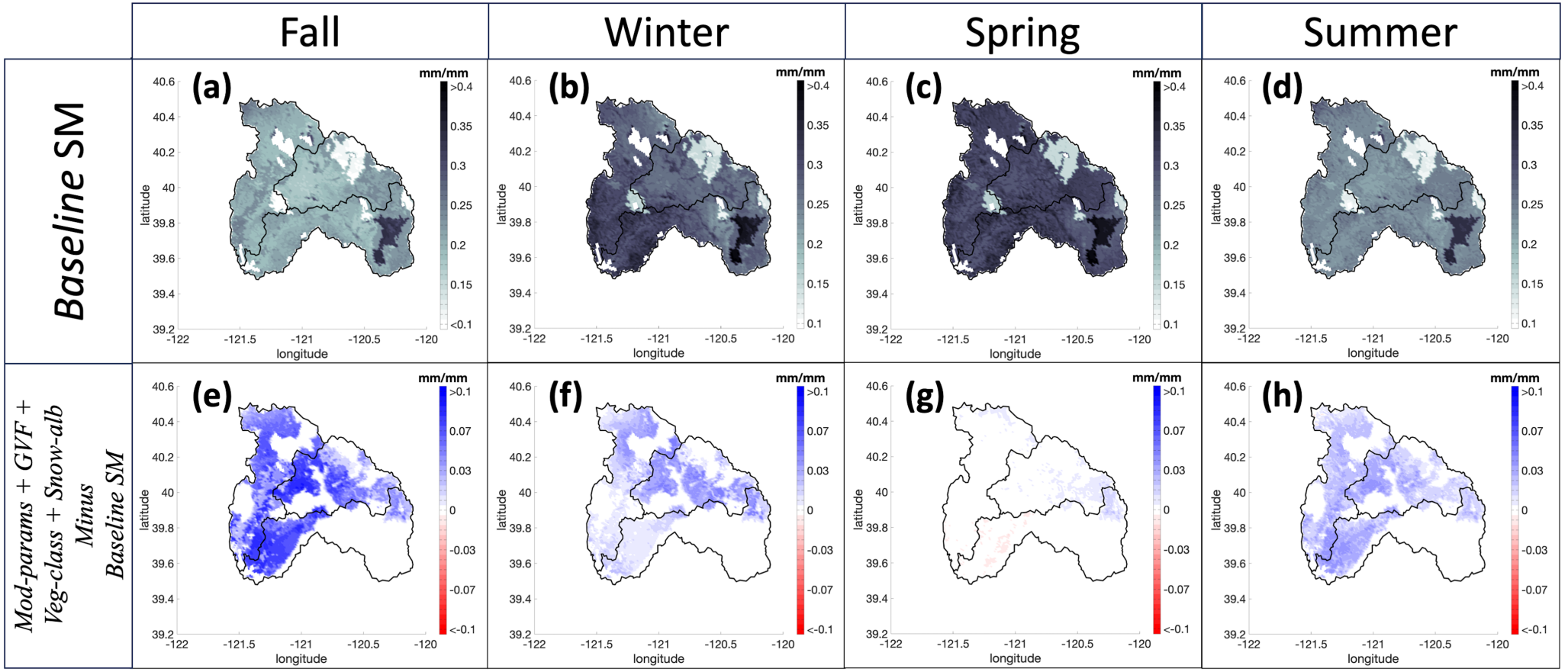

WRF-Hydro simulates fire-enhanced streamflow, reducing post-fire model anomaly biases. **(a)** perimeters of study catchments in the Feather River Basin, study gauge locations (black dots) and fire areas (red shading). **(b,c,d)** Muliyear mean (2000-2022) daily streamflow (Q) from a no-fire baseline simulation (black lines) and a fire-aware simulation (red lines) that accounts for fire impacts on soil and routing parameters, vegetation area and classifications and snow albedo; anomaly biases in black and red text are for baseline and fire-aware simulations, respectively.